Vibrational Energy Transfer in Gas Phase Water and Ammonia

Floyd Eugene Hovis, Jr.

Abstract

The V→T,R relaxation rate for $NH_3(\nu_2)$ has been studied from 198°K to 398°K by the method of laser-excited vibrational fluorescence. The self-deactivation rate constant decreases from 2.4 μsec^{-1} $torr^{-1}$ at 198°K to 0.65 μsec^{-1} $torr^{-1}$ at 398°K. The rate constants for deactivation by He, Ar, N_2, and O_2 are much smaller and show a weak temperature dependence in the opposite direction.

The vibrational relaxation rates of the coupled ν_1, ν_3 stretching level manifold and of the $2\nu_2$ bending level in $H_2{}^{18}O$ has been studied from 250°K to 400°K using the same method as for NH_3. The ν_1, ν_3 self-deactivation rate goes from 1.4 μsec^{-1} $torr^{-1}$ at 250°K to 0.48 μsec^{-1} $torr^{-1}$ at 400°K. For $2\nu_2$ it goes from 4.5 μsec^{-1} $torr^{-1}$ to 1.9 μsec^{-1} $torr^{-1}$. The temperature dependence of the deactivation of both levels by He and Ar is much weaker and the rates are several hundred times slower. Deactivation of ν_1, ν_3 by N_2, O_2, and CO_2 is measured only at 293°K. N_2 and O_2 deactivate ν_1, ν_3 about 5 and CO_2 about 50 times faster than He or Ar.

DEDICATION

To Peggy, with love

ACKNOWLEDGEMENTS

As I leave Berkeley, I find myself hoping to always be surrounded by as interesting and helpful a group of people as those I have worked with here. I want to express my appreciation to Brad Moore, my research director, for his continual support and guidance. He helped me to develop the judgment necessary to do scientific research. Linda Young, Mike Berman, and Andy Kung were of much aid in the day-to-day battle against malfunctioning equipment. Jackie Denney helped to minimize the drudgery of unavoidable paperwork, and life around the lab wouldn't have been the same without her lunch parties. Discussions with Jim Weisshaar and Hai-Lung Dai livened the days. Finally, I want to thank my wife Peggy for her patience at my absences and her constant moral support.

TABLE OF CONTENTS

CHAPTER		PAGE
I	INTRODUCTION	1
II	$NH_3(\nu_2)$ DEACTIVATION	4
	A. Introduction	4
	B. Experimental	4
	C. Result and Analysis	14
III	$H_2{}^{18}O$ DEACTIVATION STUDIES	41
	A. Introduction	41
	B. Room Temperature Measurements	42
	1. Experimental	42
	2. Kinetic Model	44
	3. Results	51
	a. Relaxation Times in Pure $H_2{}^{18}O$	51
	b. ν_1, ν_3 Quenching in Mixtures	57
	c. Relative Intensity Measurements	64
	C. Temperature Dependence of $H_2{}^{18}O$ ν_1, ν_3 and $2\nu_2$ Quenching	66
	1. Experimental	66
	2. Results and Analysis	68
IV	DISCUSSION	89
	A. Introduction	89
	B. Comparison to Other Measurements	89
	C. Comparison to Other Systems and to Theory	92
	1. H_2O and NH_3 ν_2	92
	2. H_2O (ν_1, ν_3) and H_2 ($2\nu_2$)	95

TABLE OF CONTENTS (continued)

CHAPTER			PAGE
IV	D.	Effect of Rate Constants on Laser Operation. . . .	97
	E.	Analysis of H_2O Detection Scheme	102
	F.	Implications for Planetary Atmosphere Studies. . .	107
	G.	Conclusions.	108
REFERENCES			109

CHAPTER I

INTRODUCTION

The purpose of these studies was to measure the rates of vibration-to-vibration (V→V) and vibration-to-translation and rotation (V→T,R) energy transfer in gas phase, polyatomic, hydrogen bonding systems, specifically $H_2{}^{18}O$ and NH_3. Both the temperature dependence and effect of varying collision partners was observed.

These relaxation rates are much faster than for "normal" molecules. The strong hydrogen bonding interaction and small moments of inertia are believed to be responsible for this. Table I gives the number of hard-sphere collisions, Z, required for HF, HCl, and CH_4 self-deactivation at room temperature. Note that in spite of having the least amount of energy to transfer, CH_4 is the slowest to self-deactivate.

Previous measurements of the NH_3 and H_2O V→T,R rates, primarily by ultrasonic absorption or dispersion techniques, have shown that these rates are fast; however, the measurements do not agree well in magnitude. Reported values of $NH_3(\nu_2)$ self-deactivation rates range from 4 to 35 hard-sphere collisions.[6-11] For the self-relaxation of $H_2{}^{18}O(\nu_2)$ the reported values vary between 3 and 80 hard-sphere collisions.[12-20]

By studying the temperature dependence of the relaxation rates one hopes to gain information on the mechanics and forces which cause energy transfer. The temperature dependence is an important check of theoretical models.[21]

Knowledge of these relaxation rate constants and their temperature dependences is useful for understanding more complicated systems of which they are a part. Water is a major combustion product and its vibrational

Table I

Comparison of V→T,R Self-Relaxation in HF, HCl, and CH_4

Mode Deactivated	$\nu(cm^{-1})$	Z	References
HF(v = 1)	4139	70	1, 2
HCl(v = 1)	2990	7900	3
$CH_4(\nu_4)$	1306	19,000	4, 5

relaxation affects the dynamics of the product gases. The particular pathways and rate constants for V→V and V→T,R energy transfer control the infrared laser action in electric discharge pumped water vapor.[22-25] By two-photon pumping $NH_3(2\nu_2-)$ laser action can be obtained with $1\nu_2-$ or $1\nu_2+$ as the terminal level.[26] The success of certain proposed schemes to measure the concentration of H_2O at high altitudes by looking at its ir emission will be determined by the vibrational relaxation rates of water.[27]

The method used for studying these relaxation rates is that of laser-excited vibrational fluorescence. After the molecules are initially excited to a known vibrational level, the time dependence of the ir emission from all levels of interest is monitored. By the use of an appropriate kinetic model the fluorescence intensity vs time data yields the rate constants.

CHAPTER II

$NH_3(\nu_2)$ DEACTIVATION

A. Introduction

This chapter describes the measurement of $NH_3(\nu_2)$ V→T,R relaxation rate constants as a function of collision partner and temperature. The temperatures range from 198°K to 398°K and the collision partners for which relaxation rate constants are measured are NH_3, He, Ar, N_2, and O_2.

The measurements are done by the method of laser-excited vibrational fluorescence. A CO_2 TEA laser was used to pump Q- or R-branch transitions of the $\nu_2(\pm)$ states. The time-resolved emission from the P- and Q-branches of the same level was analyzed to extract the deactivation rate constants.

B. Experimental

The CO_2 TEA laser is made from a Tachisto model 215 discharge head utilizing ZnSe Brewster angle windows to give horizontally polarized output. The oscillator cavity formed by a master grating and Ge output coupler is 120 cm long. The PTR Optics model ML-303 grating had 150 lines per mm and was blazed to give optimal first order reflectance in $E_\perp$ between 9 μm and 11 μm. This allows selection of single rotation-vibration laser transitions. With no aperture in the cavity the output beam is a rectangle of 20 mm height and 10 mm width. An adjustable iris mounted in the cavity could be used to limit the beam size. A 6 mm diameter beam giving a uniform burn pattern at the fluorescence cell was used for all experiments. The Ge output coupler was uncoated and had a 10 m radius of curvature on the cavity side and was antireflection coated and flat on the output side.

The high voltage needed for the laser excitation discharge was provided by a Hippotronics model R-50B power supply with its internal current limiting resistor removed. The discharge head itself had the necessary current limiting resistors built into the charging circuitry. The range of operating voltages was 26 kV to 30 kV. The stored energy was dumped by breaking down a spark gap built into the discharge head. This required the application of an external -200 V pulse into the discharge head circuitry. A circuit diagram of the variable rate pulser that was used is shown in Figure 1. The maximum repetition rate of the laser was two Hz, with ~ 2/3 Hz typically being used.

All of the laser components except the -200 V pulser were mounted on a 12 mm thick Al plate that was 63.5 cm x 147.5 cm. A 33 cm high box of 1.6 mm thick Al built up from this plate and was well-grounded to a Cu water pipe to help shield against RF noise generated by the laser discharge. The only holes in the box were one to allow horizontal adjustment of the grating, one to allow vertical adjustment of the output coupler, and one for laser output. To further cut down on RF noise the 110 V AC input to the high voltage power supply went through a Corcom model 3K5 EMI filter which was mounted in the wall of the Al box.

In spite of all the precautions there was ~ 2 μsec of RF pickup, most of which came before the laser pulse. This noise was found to be associated with the triggering circuitry. The -200 V pulser was external to the laser and the trigger pulses were input through a BNC connector in the wall of the laser. A small box that allowed putting varying sized capacitors between the pulser input to the laser and ground was constructed. It was found that a 1 μF capacitor greatly attenuated the RF noise but still allowed normal laser triggering at 1 Hz or less.

Figure 1. Circuit diagram for -200 V, variable repetition rate pulser used for CO_2 laser triggering.

Power Supply

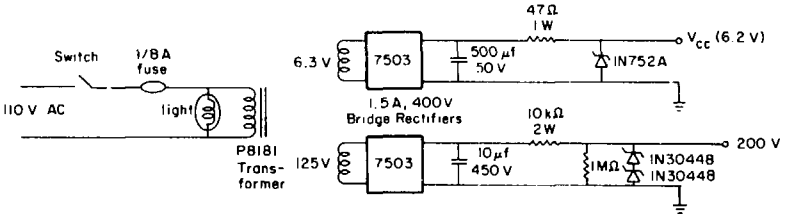

Pulse Generator

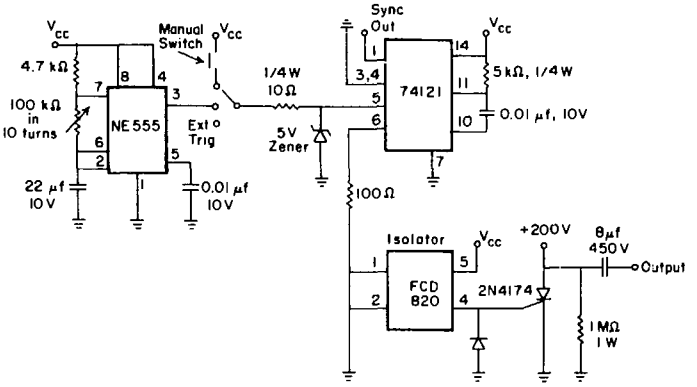

XBL 799-11653

If the $He:CO_2:N_2$ flows were adjusted to give maximum energy (flows of 16:8:6 standard cubic feet per hour) the laser pulse consists of a 50 nsec FWHM spike containing 50% of the energy followed by a ~1/2 μsec tail containing the rest. By reducing the N_2 flow and increasing the CO_2 and He flows it is possible to eliminate the tail. Running the laser on the (00°1)-(02°0) R(16) transition and using $He:CO_2:N_2$ flow rates of 12:10:3 standard cubic feet per hour gave pulses with 30-50 mJ of energy and a 50 nsec FWHM spike containing >95% of the energy. For the experiments using the (00°1)-(10°0) R(6) and (00°1)-(10°0) R(14) lines similar flow rates were used and the pulse energies varied between 35 mJ and 75 mJ. In all cases the laser pulse shapes were checked with a photon drag detector and small adjustments in the flows made to give stable output with the sharp pulses described above.

The (00°1)-(02°0) R(16) CO_2 laser transition has been shown[28] to pump the aR(6,0) line of the ν_2 fundamental vibration band of NH_3. The spectroscopic data of Shimizu[29] and Garing et al.[30] show that the (00°1)-(10°0) R(6) and R(14) laser lines pump the sQ(5,4) and aR(1,1) transitions, respectively.

The single shot signal-to-noise (S/N) was never adequate for analysis. Averaging between 100 and 200 shots gave S/N $\gtrsim$ 10. The signal averaging system consisted of a Biomation 8100 transient recorder, a Tracor-Northern NS575 or NS575A digital signal analyzer, and a Hewlett-Packard 7004B X-Y recorder. The fastest sampling rate of the transient recorder was 10 nsec per point. To establish the baseline well the sampling rate could be switched at a variable delay after the initial trigger. In most cases traces were recorded on 1/2 of the digital analyzer memory, or 1024 points. The first 800 points were recorded at

10 or 20 nsec per point and the rest at 0.5 or 1.0 μsec per point. A Rolfin model 7415 photon drag detector provided triggering for the signal averaging system as well as providing a check of the laser pulse shape in time. For the fast laser pulse used it was necessary to amplify the photon drag signal to ~1 V peak in order to get stable triggering of the transient recorder.

The infrared detector used was a liquid He cooled 5 mm x 10 mm Cu:Ge photoconductive detector. The dewar holding it and the x1 impedance matching amplifier mounted on the dewar have been described previously.[31] The detector is mounted such that the can itself provides the ground return and one lead provides the detector bias voltage and signal output. A 10 kΩ load resistor is mounted outside the Dewar in the copper box containing the x1 amplifier. A Keithley model 104 wide-band amplifier is used to amplify the signal x100 before signal averaging. The response time of the detection system using the 10 kΩ load resistor was 180 nsec.

The Dewar used has mounts for two 1" diameter substrates, one the same temperature as the detector and one liquid N_2 cooled. A 2 mm thick BaF_2 window was in the detector temperature mount and usually nothing in the liquid N_2 cooled mount. For most experiments the ir interference filters were used externally.

For the 293 ± 2°K measurements the pyrex fluorescence cell, which was 25 cm long and 2.5 cm in diameter had Brewster angle ZnSe input and output windows to minimize scattered light. The excitation beam was single passed through this cell and onto the photon drag detector. There were 2.5 cm fluorescence viewing windows of NaCl in the top and bottom of the cell. A 2.5 cm focal length parabolic mirror directed the fluorescence

coming out the bottom window back toward the detection system. A 5.1 cm diameter f/1 NaCl lens collected and focused the fluorescence onto the detector. One-to-one imaging was used.

The measurements at 198 ± 3°K and 398 ± 3°K were done with a different fluorescence cell. It was 22 cm long, 1.9 cm in diameter, and had only one fluorescence viewing window. The laser input and fluorescence viewing windows were made of 2 mm thick BaF_2. A BaF_2 rear window with a gold coating on the inner surface gave two passes of the excitation beam. All the windows were mounted with EPO-TEK H-77 high temperature epoxy. The brass, BaF_2, and epoxy all have very similar coefficients of thermal expansion, and thus minimized the chance of breaking the windows when the cell was cooled or heated. The cell and an asbestos coated steel can into which it could be mounted are shown in Figure 2. Measurements at 198 K were done by filling the dewar with a dry ice/ethanol bath. The 398 K measurements were done using a Haake model FT constant temperature circulator that had Dow Corning 550 silicone oil as the heat transfer fluid. The temperatures were measured with an Omega model UCA 35J3 calibrated thermistor. For both the 198°K and 398 K experiments dry N_2 was flowed through a Cu coil immersed in the Dewar and then over the laser input and fluorescence windows to prevent fogging and to minimize temperature gradients across the windows.

Different sets of interference filters were used for cutting out scattered light from the differing excitation lines. They are placed in metal holders which are taped directly to the base of the detector Dewar. For experiments using pumping by the (00°1)-(02°0) R(16) line two OCLI wide band pass filters were used. One of them, W11680-9, had half-power points at 770 cm^{-1} and 960 cm^{-1}, 1% transmitting points at

Figure 2. Cell used for 198°K and 398°K NH_3 measurements. The cell body is made of brass and is 22 cm long, from BaF_2 input window to rear reflector. A telescoping Cu pipe, not shown in the figure, formed a dead air space between the fluorescence window shield and the NaCl collecting lens. A 1" I.D. Cajon Ultratorr connector provides the liquid tight connection between the steel can and cell.

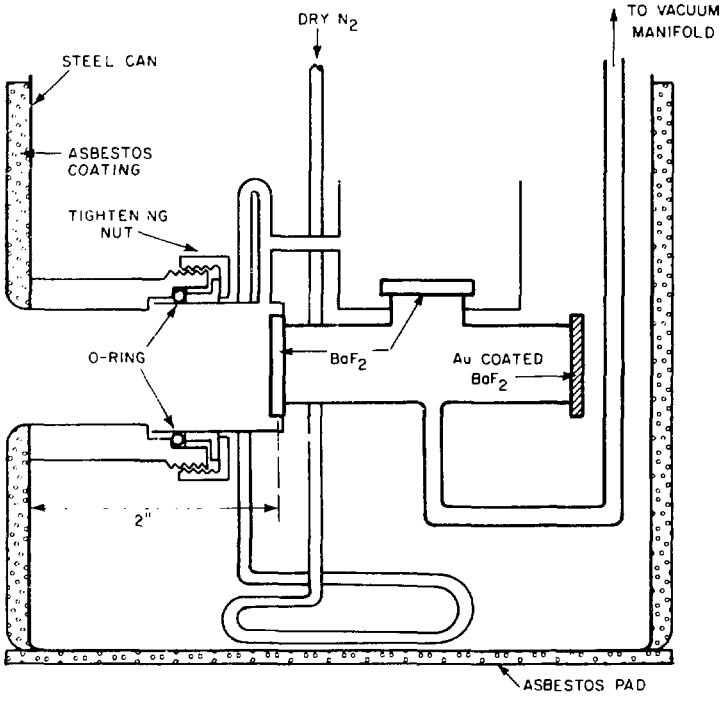

XBL 799-11654

750 cm^{-1} and 985 cm^{-1}, and ≥80% transmission from 940 cm^{-1} to 790 cm^{-1}. The other, W11724-9, had half-power points at 780 and 970 cm^{-1}, 1% transmitting points at 755 and 990 cm^{-1}, and ≥85% transmission from 795 to 950 cm^{-1}. This combination of filters transmitted most of the P- and Q-branch lines of the $NH_2(\nu_2)$ band.[30] For the experiments which used (00°1)-(10°0) R(6) and R(14) pumping, two OCLI long pass filters were used, L10832-9 and L11382-9. They had cut-on frequencies (5% transmitting) of 920 cm^{-1} and 880 cm^{-1}, respectively. The former had >75% transmission from 890 to 655 cm^{-1} and the latter had ≥85% transmission from 865 to 655 cm^{-1}. This combination transmitted most of the P-branch of the $NH_3(\nu_2)$ band. For all the experiments the liquid He cooled 2 mm BaF_2 in front of the detector eliminated frequencies less than 650 cm^{-1}.

The fluorescence cells were connected to a glass and Apiezon-N grease vacuum manifold. The manifold plus either cell could be pumped to less than 10^{-6} torr. A Celesko pressure transducer was used to measure pressures <5 torr and a Hg manometer used to measure higher pressures. To minimize uncertainties in the NH_3 pressure, the system was first saturated with NH_3 and then allowed to equilibrate until the pressure decreased less than 2% in 15 minutes. At that time the desired buffer gas was added and allowed to mix until successive traces 15 minutes apart gave the same result. This ranged from 1/2 hour for $p_T \lesssim 25$ torr to >2 hours for $p_T > 100$ torr.

The NH_3 used was Matheson anhydrous grade with a minimum purity of 99.99%. The buffer gases were Matheson research grade of the following purities: Ar, 99.9995%; He, 99.9999%; N_2, 99.999%; O_2, 99.99%. In addition, the Cu connecting line to the buffer gas tanks had a loop immersed in liquid N_2 during the course of the experiments.

C. Result and Analysis

The fundamental of the ν_2 vibration of NH_3 actually consists of two states, one which is symmetric (+) with respect to inversion and one which is asymmetric (-).[32] Since the two levels are separated by only about 35 cm^{-1} for the fundamental, their fluorescence cannot be resolved. They will be treated as a single level of 950 cm^{-1} frequency, the average of the + and - states.

Some attempts were made to do measurements in pure NH_3. It was found that the S/N of the fluorescence increased as some power of the NH_3 pressure greater than one. Four torr of NH_3 gave a S/N of ~10, but there was also long time fluorescence and shock waves due to sample heating. Figure 3 shows such a trace. This is not surprising in light of what is known about the overlap of the CO_2 laser lines with the $NH_3(\nu_2)$ absorption frequencies. The center frequencies of the laser line and absorption lines are separated by several Doppler widths[29,30] so that their coincidences are probably on the tails of the Lorentzian absorption profiles. In this case the absorption cross section will increase linearly with pressure.[33] Taking account of the simultaneously increasing number density, one would expect that the absorbed energy, and thus fluorescence, would increase as $p_{NH_3}^2$.

The sample heating can be treated in a manner similar to that used for the low frequency bends of CD_4 by Zittel and Moore.[34] An analysis similar to theirs shows that the fluorescence intensity is given by

$$F = F_0\left[\left(1 - \frac{\gamma}{1+\gamma}\right) e^{-(1+\gamma)(k_{NH_3}p_{NH_3}+k_M p_M)\,t} + \frac{\gamma}{1+\gamma}\right] \qquad (1)$$

where γ is the ratio of the heat capacity of the ν_2 mode of the NH_3 in the sample to the total heat capacity of the sample. This result assumes

Figure 3. Fluorescence intensity vs time for 3.8 torr NH_3. Note the shock wave peaks around 10 μsec and 18 μsec.

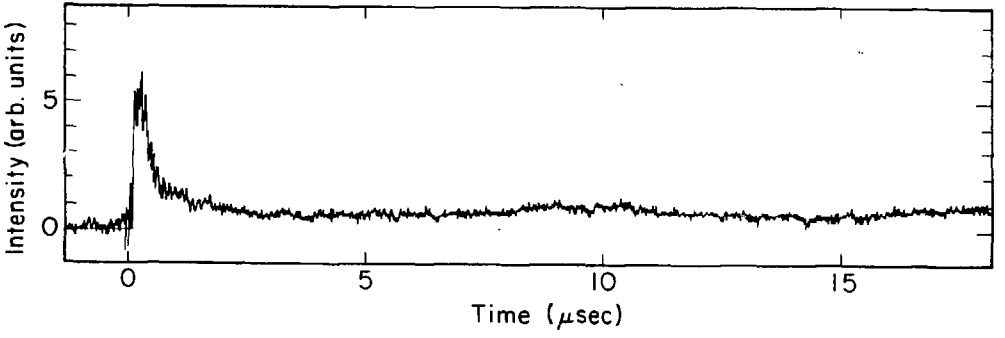

XBL 799-11852

that the V→T,R processes occur rapidly compared to energy losses out of the excitation volume, i.e., neglects heat diffusion to the walls and uses heat capacities at constant volume. It is seen that the initial intensity will decay not to zero but to $\gamma/(1+\gamma)$ of its initial value. Assuming the ν_2 mode to be a doubly degenerate harmonic oscillator at 950 cm^{-1}, $\gamma/(1+\gamma)$ is found to be about 10% for pure NH_3. An effect on the order predicted was seen in pure NH_3 samples.

The use of a buffer gas can effectively eliminate the effect just described. For an inert gas/NH_3 mixture with $X_{NH_3} = 0.05$, $\gamma/(1+\gamma)$ is only about 1%. All of the samples used to measure the relaxation rate constants have $X_{NH_3} \leq 0.05$ so the effect was negligible.

An estimate of the heating was made for a sample that should show one of the larger effects. It had $X_{NH_3} = 0.05$ with $p_{NH_3} = 0.377$ torr and $p_{Ar} = 7.55$ torr done at 293°K. For a 0.5 torr sample of pure NH_3 and laser pulse energies of 50 mJ the data of Chang and McGee on absorption of the 00°1 - 02°0 R(16) laser line[28] show that the excited volume should absorb about 0.1 mJ. Added buffer gas will increase this due to increasing the Lorentzian absorption tail. Using this 0.1 mJ figure plus empirical comparisons of pure NH_3 sample fluorescence to those with added buffer gas indicate that 0.5 mJ is a very safe upper limit on the energy absorbed by the $X_{NH_3} = 0.05$ sample. Assuming all of the absorbed energy goes into heating of only the excitation volume and using heat capacities at constant volume gives an upper limit on heating of this sample of 13°C. Nearly all of the other samples measured would have significantly less heating. Most importantly, for none of the data used were there any significant long time fluorescence tails.

To summarize this discussion, the reasons for measuring the relaxation rates in mixtures are twofold. One is that the use of a buffer gas prevents unwanted heating effects. The other is that pressure broadening by the buffer gas increases absorption on the Lorentzian tail and thus gives better S/N. Note that in the case of adding a buffer gas the heat capacity increases more rapidly than the absorbed energy so there is no runaway heating as for pure NH_3.

The method of analysis of the data is quite straight forward. Since only one excited level is involved, after the initial excitation the fluorescence intensity (and therefore excited state population) decays as a single exponential

$$F = F_0 \, e^{-t/\tau}. \tag{2}$$

The lifetime τ for a sample is measured from the slope of a plot of logF vs t. Figures 4 and 5 show a fluorescence trace and its log plot for a sample at 293 K. The lifetime is related to the parameters of interest by the equation

$$1/p\tau = (k_{NH_3} - k_M) \, X_{NH_3} + k_M \tag{3}$$

where p is the total pressure, k_{NH_3} the NH_3 self-deactivation rate constant, k_M the buffer gas deactivation rate constant, and X_{NH_3} the mole fraction of NH_3. By plotting $1/p\tau$ vs X_{NH_3} for a series of mixtures with M, k_{NH_3} and k_M are given by the slope and intercept.

For a given temperature it was not necessary to do a full $1/p\tau$ vs X_{NH_3} plot for all the buffer gases studied. Initially, such a set of data would be taken for one or two of the buffer gases. The value of k_{NH_3} and the appropriate k_M was obtained by linear least squares fits of

Figure 4. Trace of fluorescence intensity vs time for an Ar/NH_3 mixture at 293°K.

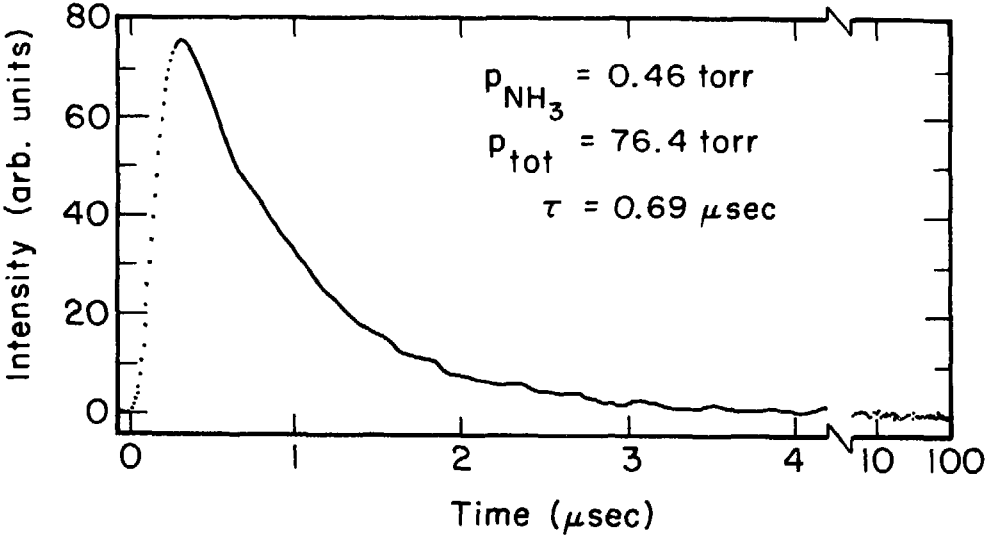
80
60
40
20
0
Intensity (arb. units)
p_{NH_3} = 0.46 torr
p_{tot} = 76.4 torr
τ = 0.69 μsec
0
1
2
3
4
10
100
Time (μsec)

XBL 786-9284

Figure 5. Trace of log of fluorescence intensity vs time for data of Figure 4.

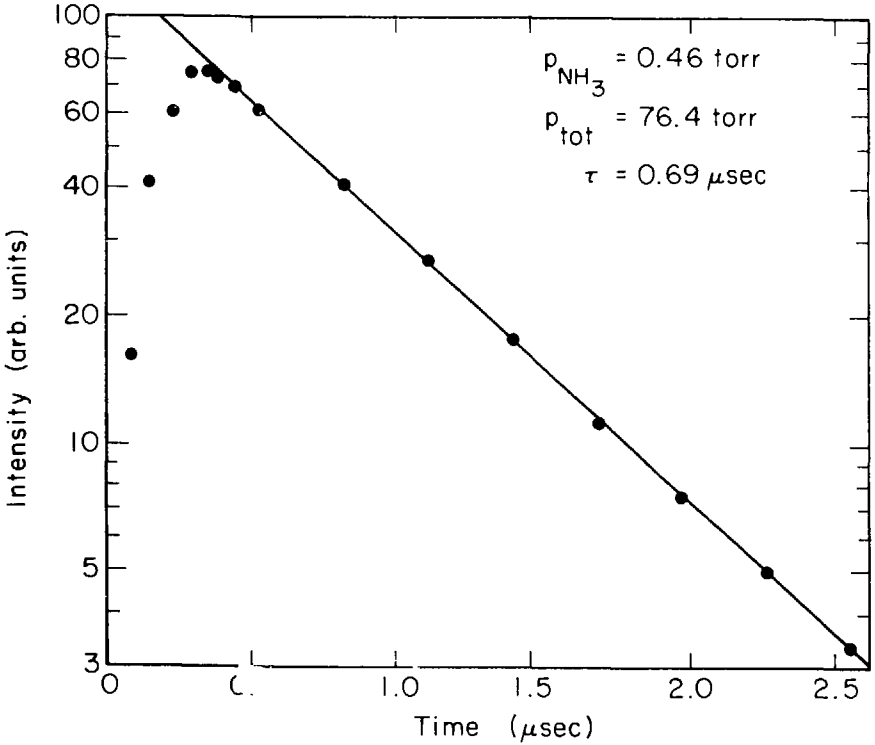
p_{NH_3} = 0.46 torr
p_{tot} = 76.4 torr
τ = 0.69 μsec
Intensity (arb. units)
100
80
60
40
20
10
5
3
0
1.0
1.5
2.0
2.5
Time (μsec)

XBL 786-9217

the data in which each point is weighted by $1/\sigma_i$, with $\sigma_i \propto (1/p\tau_i)$. For the rest of the buffer gases only data at low X_{NH_3} were taken. The value of k_M was calculated from each mixture using Equation (3) and the results of 4 to 7 mixtures averaged to give the reported value for k_M.

In estimating the uncertainties of the $NH_3(\nu_2)$ deactivation rate constants, account was taken of the effect of possible systematic errors in the NH_3 pressure. For all of the k_{NH_3}'s the standard deviations estimated from the least squares fits were 4% or less. To take account of the effect of NH_3 pressure uncertainties on k_{NH_3} we note that for the high mole fraction points that are the most important, $k_{NH_3} \sim 1/p\tau X_{NH_3}$. The random uncertainty in the $1/p\tau$ values is estimated to be 5%. The uncertainty in X_{NH_3} (i.e., in p_{NH_3}) is estimated to be 10%. This estimate is gotten from H_2O experiments where it was possible to measure the self-relaxation in pure H_2O and in mixtures. The rate constants from pure samples and from mixtures were compared. This showed that 10% is a reasonable estimate of the possible error caused in X_{H_2O} due to adsorption or desorption of H_2O when the buffer gas was added. Since the effect should be no larger for NH_3, 10% was also used as the uncertainty in X_{NH_3}. Using this plus the 5% $1/p\tau$ uncertainty gives a ±15% uncertainty in k_{NH_3}.

The uncertainties in the k_M's were estimated using $k_M = 1/p\tau - k_{NH_3} X_{NH_3}$ since in all cases $k_M << k_{NH_3}$. This gives

$$\Delta k_M = \Delta(1/p\tau) + \Delta(k_{NH_3} X_{NH_3}). \tag{4}$$

For each mixture from which a k_M was calculated a Δk_M was estimated using 5% of the $1/p\tau$ value for $\Delta(1/p\tau)$ and 25% of the $k_{NH_3} X_{NH_3}$ value as the $\Delta(k_{NH_3} X_{NH_3})$. This procedure takes account of the effect possible

systematic errors in k_{NH_3} and X_{NH_3} could have on the k_M's. The uncertainty reported for a given k_M is the average of the Δk_M's. In the case of k_M's gotten from least squares fits, the lowest X_{NH_3} points were used to estimate the Δk_M's as just described.

The data for determining k_{NH_3} as a function of temperature are shown in the $1/p\tau$ vs X_{NH_3} plots of Figures 6-9. While taking the 198°K and 293°K data a check was made to see if any dependence of the relaxation rates on rotational state could be observed. If there were such an effect it would most likely be observed at higher X_{NH_3} values where there is less rotational relaxation by the buffer gas. At 198°K using N_2 as the buffer gas no effect is observed, as illustrated in Figure 6. Some additional measurements with Ar at 293°K, not shown in Figure 8 were also done. A sample with p_{NH_3} = 0.377 torr, p_{Ar} = 7.17 torr and thus X_{NH_3} = 0.50 was studied using all three of the possible excitation lines. Using the previously measured k_{Ar}, all of the measured τ's gave values of k_{NH_3} that agreed with the value from Figure 8 within 10%. Since the S/N for these experiments is not as good as for much of the data, this difference is not significant.

To be sure that the observed fluorescence was due to ν_2 fundamental and not hot band fluorescence, an experiment was done with a 4 cm gas filter cell containing ~ 170 torr of NH_3 between the fluorescence cell and detector. The peak fluorescence intensity seen with NH_3 in the filter cell was about 3% of that seen with the cell empty for a sample containing 0.67 torr of NH_3 and 66 torr of Ar. Thus population of higher levels is not sufficient to interfere with the ν_2 fundamental fluorescence analysis.

Figure 6. $NH_3(\cdot_2)$ deactivation in mixtures with N_2 at 198°K and 398°K. The x's are at 398°K using (00°1)-(02°0)R(16) excitation, and give a slope of 0.65 μsec^{-1} $torr^{-1}$ and an intercept of 0.011 μsec^{-1} $torr^{-1}$. The solid points are at 198°K and give a slope of 2.3 μsec^{-1} $torr^{-1}$ and an intercept of 0.0091 μsec^{-1} $torr^{-1}$. The excitation lines for the 198°K data are: ● - (00°1)-(02°0) R(16); ■ - (00°1)-(10°0) R(6); and ▲ - (00°1)-(10°0) R(14).

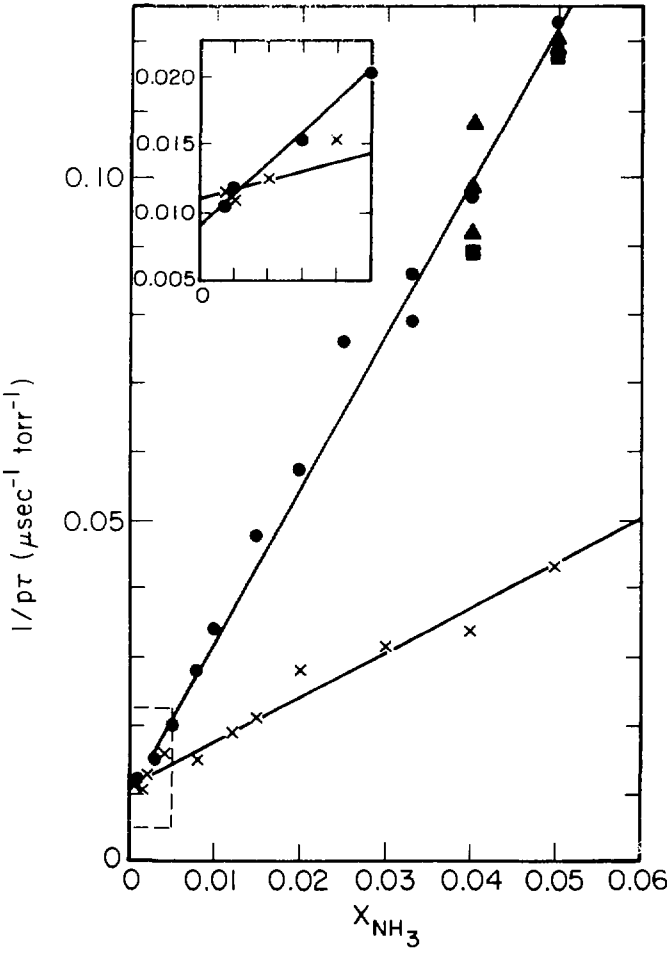

XBL 799-11655

Figure 7. $NH_3(v_2)$ deactivation in mixtures with He at 198°K using (00°1)-(10°0) R(14) excitation. The slope is 2.5 μsec^{-1} $torr^{-1}$ and the intercept is 0.0056 μsec^{-1} $torr^{-1}$.

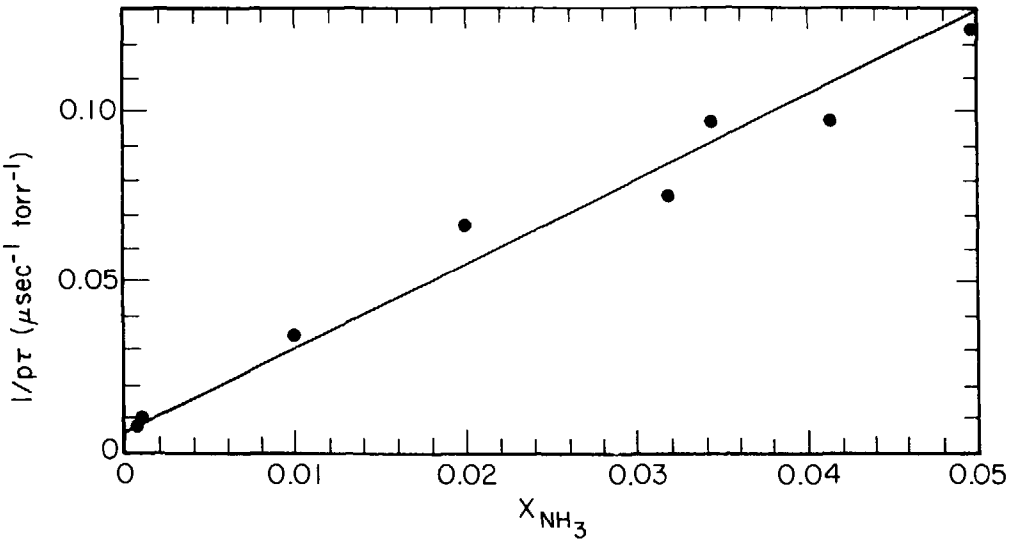

XBL 799-11656

Figure 8. $NH_3(\nu_2)$ deactivation in mixtures with Ar at 293°K using (00°1)-(02°0) R(16) excitation. The slope is 1.3 μsec^{-1} $torr^{-1}$ and the intercept is 0.0059 μsec^{-1} $torr^{-1}$.

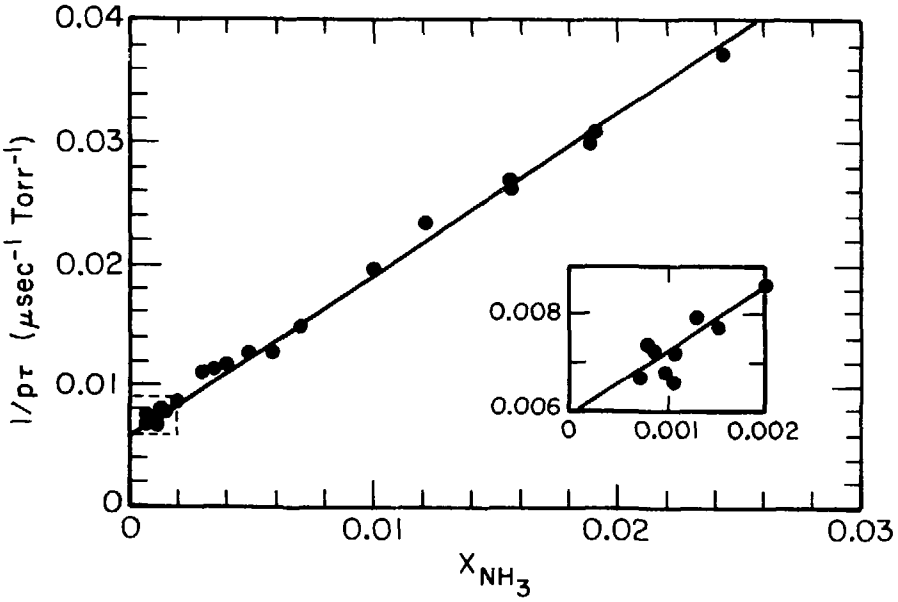

XBL 799-11658

Figure 9. $NH_3(\nu_2)$ deactivation in mixtures with He at 293°K using (00°1)-(02°0) R(16) excitation. The slope is 1.2 μsec^{-1} $torr^{-1}$ and the intercept is 0.0093 μsec^{-1} $torr^{-1}$.

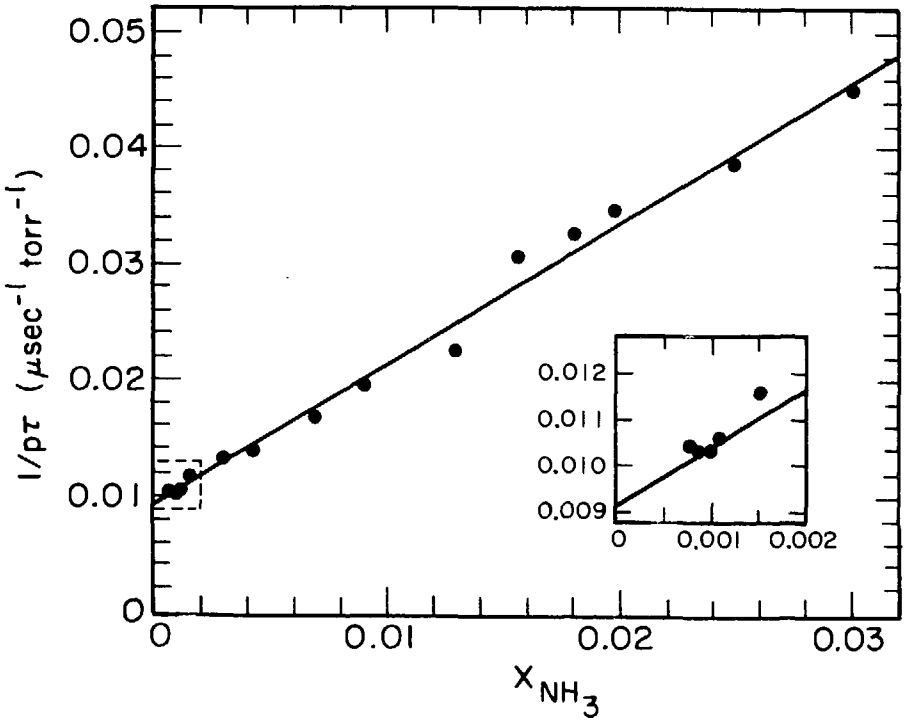
0.05
0.04
0.03
0.02
0.01
0
$1/p\tau$ (μsec^{-1} $torr^{-1}$)
0
0.01
0.02
0.03
X_{NH_3}
0.012
0.011
0.010
0.009
0
0.001
0.002

XBL 786-9283

The low X_{NH_3} data from which the remaining k_M's were determined are shown in Figures 10-12. The NH_3 pressures used ranged between 0.08 torr and 0.25 torr and the X_{NH_3}'s between 0.00066 and 0.029. The lines drawn on the figures have a slope equal to the average value of k_M from all mixtures and an intercept of zero.

A summary of all the measured $NH_3(\nu_2)$ deactivation rate constants along with their corresponding cross sections and probabilities is given in Table II.

Figure 10. Data for $NH_3(\nu_2)$ deactivation by Ar and O_2 at 198°K.

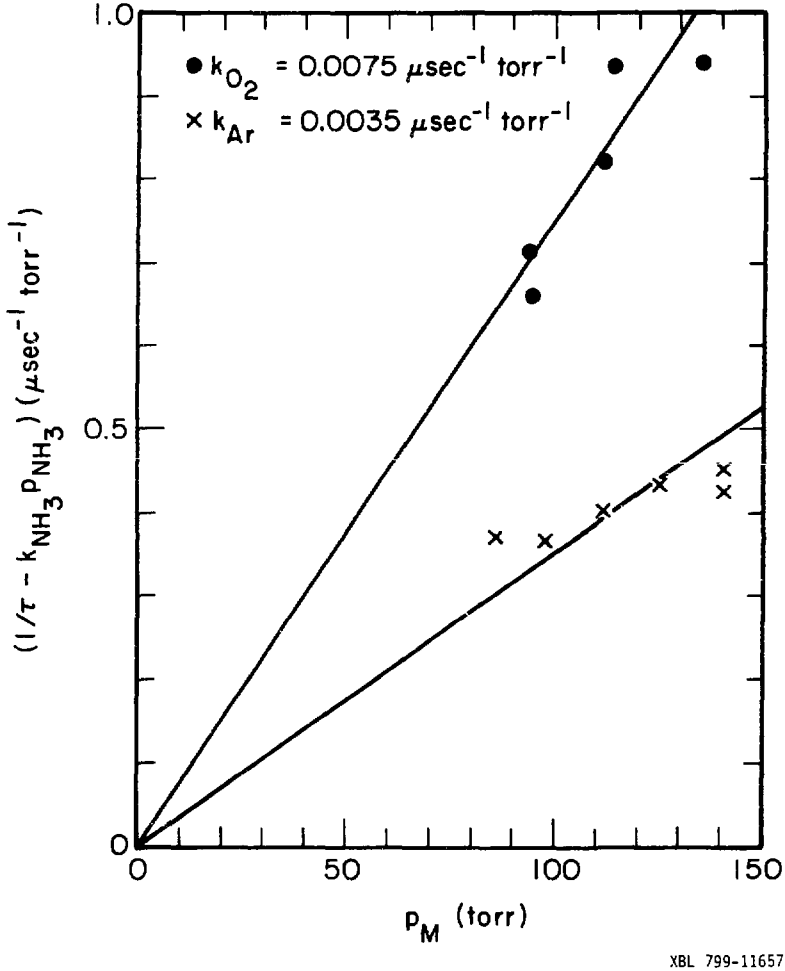

XBL 799-11657

Figure 11. Data for $NH_3(\nu_2)$ deactivation by O_2 and N_2 at 293°K.

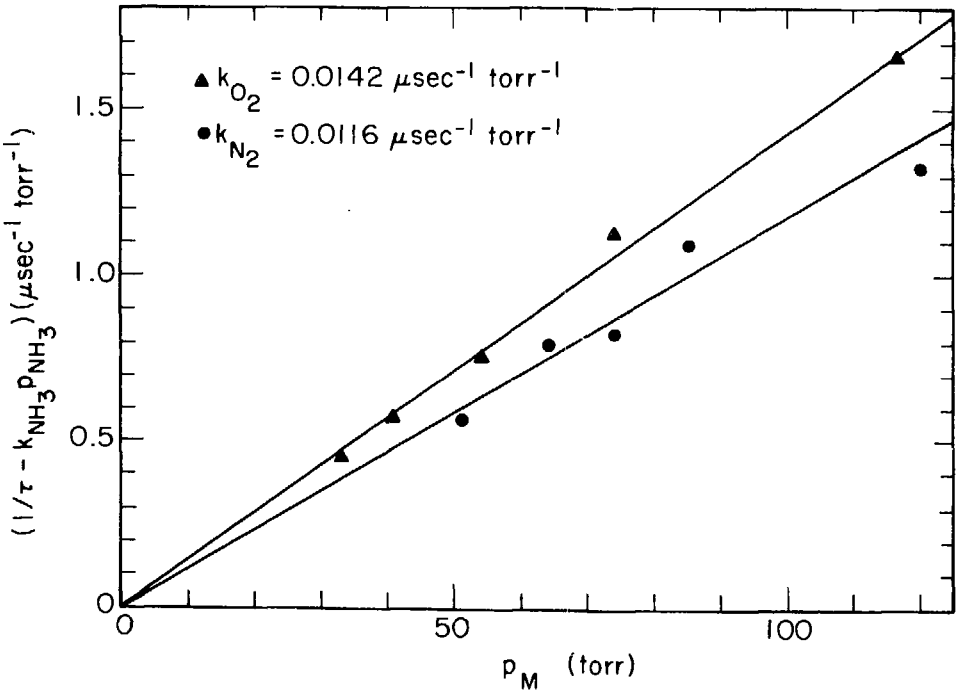
▲ k_{O_2} = 0.0142 μsec^{-1} $torr^{-1}$
● k_{N_2} = 0.0116 μsec^{-1} $torr^{-1}$
$(1/\tau - k_{NH_3} p_{NH_3})$ (μsec^{-1} $torr^{-1}$)
1.5
1.0
0.5
0
0
50
100
p_M (torr)

XBL 786-9286

Figure 12. Data for $NH_3(\nu_2)$ deactivation by He, Ar, and O_2 at 398°K.

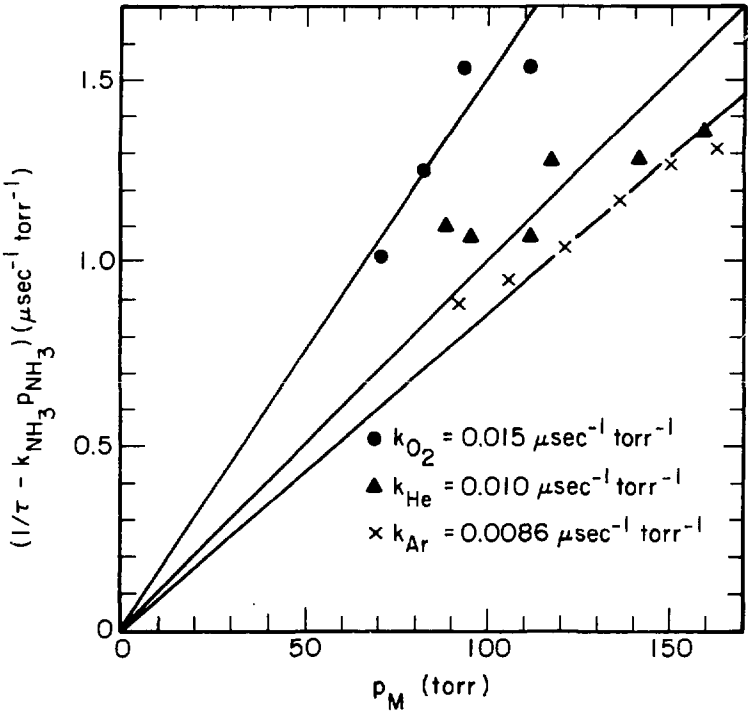

XBL 799-11659

Table II

Deactivation of $NH_3(v_2)$ by M

M	T(°K)	k(μsec^{-1} $torr^{-1}$)	k(cm^3 $molecule^{-1}$ sec^{-1})	$\bar{\sigma}(Å^2)$[a]	P^a
NH_3	198	2.4 ± 0.4	$(4.9 \pm 0.7) \times 10^{-11}$	6.9	0.22
	293	1.3 ± 0.2	$(3.8 \pm 0.6) \times 10^{-11}$	4.4	0.14
	398	0.65 ± 0.10	$(2.7 \pm 0.4) \times 10^{-11}$	2.7	0.085
He	198	$(5.6 \pm 1.0) \times 10^{-3}$	$(1.1 \pm 0.2) \times 10^{-13}$	0.010	4.4×10^{-4}
	293	$(9.3 \pm 1.0) \times 10^{-3}$	$(2.8 \pm 0.3) \times 10^{-13}$	0.020	8.8×10^{-4}
	398	$(1.0 \pm 0.15) \times 10^{-2}$	$(4.1 \pm 0.6) \times 10^{-13}$	0.025	11×10^{-4}
Ar	198	$(3.5 \pm 1.0) \times 10^{-3}$	$(0.7 \pm 0.2) \times 10^{-13}$	0.012	4.2×10^{-4}
	293	$(5.9 \pm 0.7) \times 10^{-3}$	$(1.8 \pm 0.2) \times 10^{-13}$	0.025	8.7×10^{-4}
	398	$(8.6 \pm 0.7) \times 10^{-3}$	$(3.6 \pm 0.3) \times 10^{-13}$	0.043	15×10^{-4}
N_2	198	$(9.1 \pm 1.4) \times 10^{-3}$	$(1.9 \pm 0.3) \times 10^{-13}$	0.030	9.5×10^{-4}
	293	$(1.2 \pm 0.13) \times 10^{-2}$	$(3.6 \pm 0.4) \times 10^{-13}$	0.047	15×10^{-4}
	398	$(1.1 \pm 0.1) \times 10^{-2}$	$(4.5 \pm 0.4) \times 10^{-13}$	0.050	16×10^{-4}
O_2	198	$(7.5 \pm 1.2) \times 10^{-3}$	$(1.5 \pm 0.25) \times 10^{-13}$	0.025	8.6×10^{-4}
	293	$(1.4 \pm 0.14) \times 10^{-2}$	$(4.2 \pm 0.4) \times 10^{-13}$	0.056	19×10^{-4}
	398	$(1.5 \pm 0.12) \times 10^{-2}$	$(6.1 \pm 0.5) \times 10^{-13}$	0.070	24×10^{-4}

[a]Calculated using the molecular diameters d_{NH_3} = 3.17 Å, d_{He} = 2.24 Å, d_{Ar} = 2.86 Å, d_{N_2} = 3.15 Å and d_{O_2} = 2.93 Å. $\bar{\sigma} = k/\bar{v}$.

CHAPTER III

$H_2{}^{18}O$ DEACTIVATION STUDIES

A. Introduction

The experiments described in this chapter are studies of the V→V and V→T,R relaxation rates of $H_2{}^{18}O$ using the method of laser-excited vibrational fluorescence. The first set to be described was done at room temperature using a relatively low power Nd:YAG pumped optical parametric oscillator (OPO) to provide tunable ir with which the asymmetric stretch, ν_3, could be excited. Fluorescence is observed from the coupled ν_1, ν_3 stretching manifold, from the bend overtone $2\nu_2$, and from the bend fundamental ν_2.

There are a number of purposes for the room temperature studies. The first was to provide more data for the calculation of the total deactivation rates of the vibrational levels involved. Much data on this had already been taken by Finzi.[31] In addition, measurements of the relative fluorescence intensities from $2\nu_2$ and ν_2 were done and analyzed to give qualitative information on the branching ratios of the various V→V pathways. Finally, measurements of the quenching of the stretching levels by N_2, O_2, and CO_2 were made because of their importance in atmospheric problems. All of these are described in Section B of this chapter.

Section C of this chapter describes studies of the temperature dependence of the total deactivation rates of ν_1, ν_3 and $2\nu_2$ from 250°K to 400°K. A newer more powerful Nd:YAG pumped OPO was used to make these measurements.

B. Room Temperature Measurements

1. Experimental

Most of the experimental set-up has been described previously,[31] and only a summary of the most important features will be given here.

Because of the difficulty in trying to eliminate atmospheric $H_2{}^{16}O$ from the OPO cavity, $H_2{}^{18}O$ was used for these experiments. The vibrational frequencies[35,36] of $H_2{}^{16}O$ and $H_2{}^{18}O$ for the levels of interest differ at most by 15 cm^{-1}, implying that their vibrational energy transfer rates should be similar.

A Chromatix model 1000E Nd:YAG laser was used to pump the 90 phase-matched, temperature-tuned, OPO. A Fabry-Perot etalon with a free spectral range of 1.4 cm^{-1} and a finesse of 14 at 3850 cm^{-1} was used in the OPO cavity. This increased the power per cavity mode and the frequency stability. In addition, since only one cavity mode overlaps an absorption line and that one is essentially completely absorbed, decreasing the power and number of nonabsorbing modes decreases the scattered light. The etalon restricts oscillation to less than four cavity modes spaced by 0.025 cm^{-1}. The OPO output near 3800 cm^{-1} consisted of 70-100 nsec pulses (FWHM) at either 45 or 75 Hz and 5-10 μJ in energy. Roughly 15% of the beam was split off and sent through a spectrophone cell containing 4 torr of water vapor to allow continuous monitoring of the water vapor excitation. Finzi's previous results[31] had found no dependence of the relaxation rates on the initially excited rotational state. Therefore, all measurements looking at $2\nu_2$ or ν_2 were done exciting on the strongest ν_3 line at 3839.8 cm^{-1}. For the experiments observing ν_3 fluorescence, excitation was on the ν_3 line at 3730.6 cm^{-1}. The assignments of these transitions have been given by Fraley et al.[35] All experiments were done at 20 ± 2°C.

The signal averaging system was the same as that used for the NH_3 experiments described in Chapter II.

The infrared detector was a 3 mm x 10 mm Cu:Ge photoconductive detector cooled to 14°K. In conjunction with an SBRC model A320 current feedback amplifier it had a risetime of 80 nsec. The Dewar containing the detector had a liquid N_2 cooled, rotatable filter wheel capable of holding up to six 2.5 cm diameter interference filters. An additional filter was placed outside the detector Dewar. For observation of $\nu_2(v_2 = 1 \rightarrow 0)$ or $2\nu_2(v_2 = 2 \rightarrow 1)$ fluorescence a long wavelength pass filter with a 2000 cm^{-1} cut-on was used externally. A wide pass filter with FWHM of 600 cm^{-1} centered at 1500 cm^{-1} was used inside. For observation of ν_3 fluorescence a short pass filter with a cut-on of 3750 cm^{-1} was used externally. A wide pass filter with a FWHM of 1100 cm^{-1} centered at 4290 cm^{-1} was used inside. A 5 cm diamter f/1 CaF_2 lens focused light from the fluorescence cell onto the detector.

The fluorescence cell was rectangular with reflecting mirrors of ThF_2-overcoated silver to allow multiple passing of the excitation beam. The fluorescence transmitting windows were made of CaF_2. The combined leak rate of the fluorescence cell and glass and Apiezon-N grease vacuum manifold was $<5 \times 10^{-4}$ torr per hour. The space between the fluorescence cell and detector was purged with dry N_2. A 4.4 cm long gas filter containing about 20 torr of water vapor was inserted in this space to block ν_2 fluorescence for observation of $2\nu_2$ fluorescence alone.

For experiments in which relative fluorescence intensities were measured the 4.4 cm filter cell was replaced by a 15 cm long evacuable filter cell that also held the collecting lens. It filled all but 5 mm of the distance between the fluorescence cell and detector. The lens

holder/filter cell was first evacuated and the total ν_2 plus $2\nu_2$ fluorescence was observed. Then it was filled with 13 torr of $H_2{}^{18}O$ and the $2\nu_2$ fluorescence alone was observed under identical conditions. Only pairs of traces for which the amplitude of the spectrophone cell signal varied by less than 7% from the mean value were used. After both traces were taken the $H_2{}^{18}O$ in the lens holder/filter cell was frozen out and the cell re-evacuated before the next pair of traces was taken.

The strong adsorption of water vapor on surfaces requires special care in pressure measurements. For pure H_2O a Celesko pressure transducer continuously monitored the pressure. Only data for which the pressure changed <2% were used. For mixture experiments, the partial pressure of water vapor was held constant by equilibration with water in a cooled sidearm whose temperature was controlled to ±0.05°C. The partial pressures of the H_2O in the various mixtures ranged between 0.28 and 0.43 torr.

The $H_2{}^{18}O$ used was distilled from a sample that was >95% ^{18}O water and that had been degassed in three freeze-thaw cycles. The other gases used were of the same purity as those given in Chapter II.

2. Kinetic Model

The energy levels involved are shown in Figure 13. The rate processes involved and the derivation of the needed equations will be summarized in this section.

For $H_2O(\nu_2)$, level 1, there is only one deactivation channel

$$H_2O(\nu_2) + M \xrightarrow{k_{10}} H_2O(0) + M + 1588\ cm^{-1} \qquad (5)$$

where M is any collision partner, including H_2O. $H_2O(2\nu_2)$ may be deactivated by

Figure 13. Energy level diagram for $H_2{}^{18}O$. Laser excitation (heavy) and fluorescence are indicated by vertical arrows.

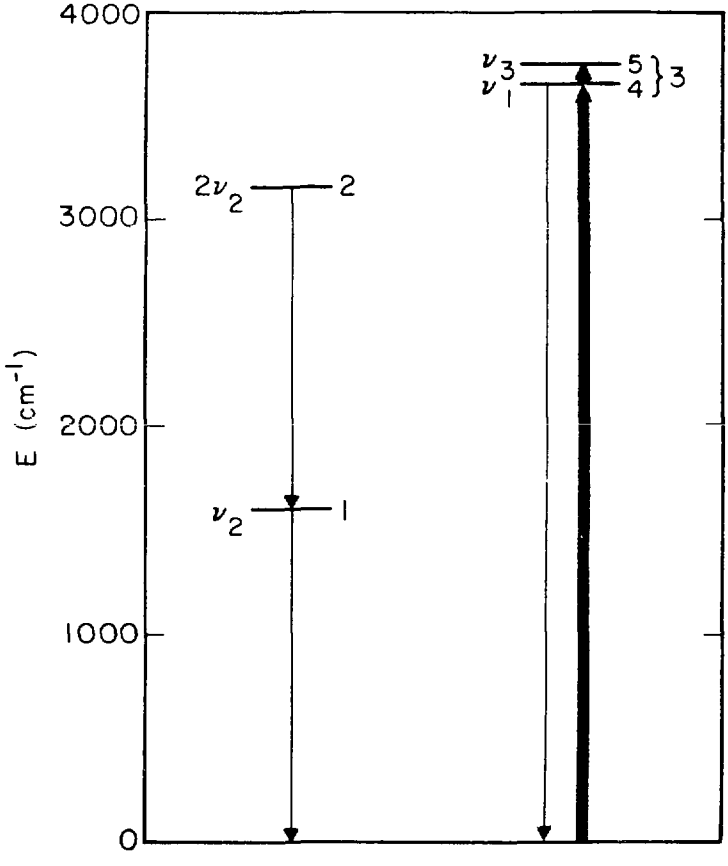

XBL 799-11662

$$H_2O(2\nu_2) + H_2O(0) \xrightarrow{k_{21}} 2H_2O(\nu_2) - 31\ cm^{-1} \tag{6}$$

$$H_2O(2\nu_2) + M \xrightarrow{k'_{21}} H_2O(\nu_2) + M + 1557\ cm^{-1} \tag{7}$$

$$H_2O(2\nu_2) + M \xrightarrow{k_{20}} H_2O(0) + M + 3145\ cm^{-1}. \tag{8}$$

The stretching levels can transfer energy to any of the lower levels

$$H_2O(stretch) + M \xrightarrow{k_{i2}} H_2O(2\nu_2) + M + 596\ cm^{-1} \tag{9}$$

$$H_2O(stretch) + H_2O(0) \xrightarrow{k_{i1}} 2H_2O(\nu_2) + 565\ cm^{-1} \tag{10}$$

$$H_2O(stretch) + M \xrightarrow{k'_{i1}} H_2O(\nu_2) + M + 2153\ cm^{-1} \tag{11}$$

$$H_2O(stretch) + M \xrightarrow{k_{i0}} H_2O(0) + M + 3741\ cm^{-1}. \tag{12}$$

The value of i indicates which stretching level is involved with i = 4 implying ν_1, i = 5 implying ν_3, and i = 3 implying the two stretching levels treated as a reservoir. The ΔE's given are for ν_3 and would be 92 cm^{-1} less for ν_1. Since the band centers of ν_1 and ν_3 are separated by only 92 cm^{-1}, energy transfer may occur in both directions

$$M + H_2O(\nu_3) \underset{k_{45}}{\overset{k_{54}}{\rightleftharpoons}} H_2O(\nu_1) + M + 92\ cm^{-1} \tag{13}$$

Except for (13) all processes are considered to proceed in the forward direction only. This follows from the large energy discrepancies and/or small populations of excited molecules. All radiative decay rates are at least three orders of magnitude slower than the measured

collisional decay rates and are neglected.[37,38]

From processes (5)-(13) first order differential rate equations may be written for each level $N_i(t)$. This is done in two parts. First, the coupled equations describing ν_1 and ν_3 are solved to give their time dependence. Then assuming ν_1 and ν_3 act as a single reservoir the time dependences of $2\nu_2$ and ν_2 are obtained. For all of the analyses it is assumed that the excited population is small so that the ground state population can be treated as constant.

The equations for the stretching levels are simplified by defining

$$k_3 = (k_4 + \beta k_5)/(1+\beta)$$

$$k_3^* = (k_5 + \beta k_4)/(1+\beta)$$

$$k_4 = k_{42} + k_{41} + k_{41}' + k_{40}$$

$$k_5 = k_{52} + k_{51} + k_{51}' + k_{50}$$

$$\beta = k_{45}/k_{54} = \exp[-(92\ \mathrm{cm}^{-1})hc/kT] = 0.64. \tag{14}$$

Solving the coupled differential equations implied by (9)-(13) for excitation of level 5 gives

$$N_5(t) = \frac{N_5(0)}{1+\beta}\left\{\beta e^{-r_1 t} + e^{-r_2 t}\right\} \tag{15}$$

$$N_4(t) = \frac{N_5(0)}{1+\beta}\left\{e^{-r_1 t} - e^{-r_2 t}\right\} \tag{16}$$

$$N_3(t) = N_4(t) + N_5(t) = N_5(0)\ e^{-r_1 t} \tag{17}$$

where

$$r_1 = k_3[H_2O]$$

$$r_2 = (k_{54} + k_{45} + k_3^*)[H_2O]. \tag{18}$$

Notice that k_3 is simply the weighted average of the rate constants for deactivation of ν_1 and ν_3. In deriving (15) and (16) the assumption that $(k_5 - k_4)^2 << 6.5\ k_{54}\ k_3$ was made. The basis for this assumption is as follows. Without making the assumption one finds that

$$r_{\substack{2\\1}} = \frac{[H_2O]}{2}\ \{k_5+k_4+k_{54}+k_{45} \pm (k_{54}+k_{45})(1+x)^{\frac{1}{2}}\}$$

where

$$x = \frac{2(k_{54}-k_{45})(k_5-k_4)}{(k_{54}+k_{45})^2} + \frac{(k_5-k_4)^2}{(k_{54}+k_{45})^2}\ .$$

Expanding $(1+x)^{\frac{1}{2}}$ as a power series in x gives for r_1

$$r_1 = [H_2O]\left(k_3 - \frac{(k_5-k_4)^2}{4k_{54}(1+\beta)} + \frac{(k_5-k_4)^2(1-\beta)^2}{4k_{54}(1+\beta)^3} + \begin{matrix}\text{higher}\\ \text{order}\\ \text{terms}\end{matrix}\right). \tag{19}$$

Clearly the 2nd term in (19) is larger than the 3rd. From the observations[31] that: (1) the ν_1, ν_3 fluorescence decays as a single exponential of the same rate whether ν_1 or ν_3 is excited and (2) the ν_3 fluorescence is smaller relative to the bending fluorescence than expected it is concluded that $\nu_1 - \nu_3$ coupling is rapid and a lower limit on k_{54} of 10 μsec^{-1} $torr^{-1}$ is estimated. In addition, k_5 and k_4 are expected to be similar in magnitude and as will be shown later $k_3 = (k_4 + k_5)/(1+\beta) = 0.75\ \mu sec^{-1}\ torr^{-1}$. Thus a reasonable assumption is $(k_5-k_4)^2/4k_{54}(1+\beta) << k_3$, yielding Equation (18).

The time dependence of the $2\nu_2$ population follows from Equations (6)-(8) and (17):

$$N_2(t) = C_2\left(e^{-k_3[H_2O]t} - e^{-k_2[H_2O]t}\right) \tag{20}$$

where

$$k_2 \equiv (k_{21}+k'_{21}+k_{20})$$

$$C_2 \equiv N_5(0)[k_{32}/(k_2-k_3)].$$

The rate constant k_2 gives the total deactivation rate of $2\nu_2$. The rate constant k_{32} is for overall transfer from the stretching reservoir to $2\nu_2$, the population weighted average of the $\nu_1 \rightarrow 2\nu_2$ and $\nu_3 \rightarrow 2\nu_2$ rate constants.

The time dependence of $N_1(t)$ is

$$N_1(t) = C_1C_2\left[Ae^{-k_3[H_2O]t} + Be^{-k_2[H_2O]t} - (A+B)\, e^{-k_1[H_2O]t}\right] \tag{21}$$

where

$$C_1 \equiv (2k_{21} + k'_{21})$$

$$A \equiv [1 + W(k_2-k_3)/C_1]/(k_1-k_3)$$

$$W \equiv (2k_{31} + k'_{31})/k_{32}$$

$$B = (k_2 - k_1)^{-1}.$$

The rate constant $k_1 \equiv k_{10}$ gives the total decay rate of ν_2. The rates for transfer from the stretching reservoir to give $2H_2O(\nu_2)$ or $H_2O(\nu_2)$ + $H_2O(0)$ are given by k_{31} and k'_{31}, respectively. These are population - weighted averages of the corresponding rate constants for ν_1 and ν_3.

The quantity W/2 is the ratio of the number of bending quanta produced directly in ν_2 to those produced via $2\nu_2$.

The ratio F of the integrated fluorescence from ν_2 to that from $2\nu_2$ is measured experimentally. Since the geometry, detector sensitivity, and filter transmission factors are nearly identical for $\nu_2 = 2 \rightarrow 1$ and $\nu_2 = 1 \rightarrow 0$ fluorescence,

$$F = \left(\frac{1}{\tau_1}\right) \int_0^\infty N_1(t)dt \Big/ \left(\frac{1}{\tau_2}\right) \int_0^\infty N_2(t)dt$$

$$= \left(\frac{\tau_2}{\tau_1}\right) (C_1 + k_2 W)/k_1 \qquad (22)$$

where τ_1 and τ_2 are the radiative lifetimes for ν_2 and $2\nu_2$. The value of F gives qualitative information on the channels through which energy flows.

3. Results

a. Relaxation Times in Pure $H_2{}^{18}O$

Since $H_2{}^{18}O(\nu_3)$ has a radiative decay about 14 times[37] that of $H_2O(\nu_1)$, the fluorescence from the stretching region is due almost entirely to the ν_3 population. However, the double exponential predicted by Equation 15 is never observed. Finzi et al.[31,39] show that this is due to the fact that the equilibration of ν_1 and ν_3 occurs faster than the time response of the ir detector. They set a lower limit for k_{54} of 10 μsec^{-1} torr. The single exponential decays of ν_3 fluorescence observed are thus a measure of k_3.

The measured decay times for the stretching vibrations from Finzi's data[31] plus these experiments are plotted in Figure 14. The slope of this plot gives $k_3 = (7.5 \pm 0.7) \times 10^5$ sec^{-1} $torr^{-1}$. Uncertainties quoted are the standard deviations for a single measurement.

Figure 14. Inverse decay time vs pressure from $H_2{}^{18}O(\nu_3)$ fluorescence experiments.

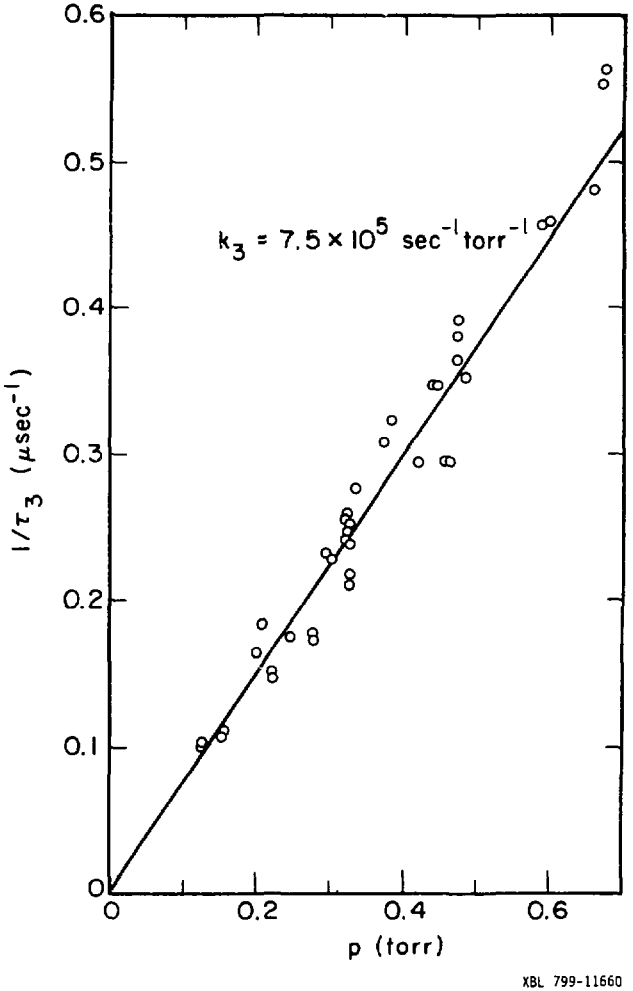

XBL 799-11660

The $2\nu_2$ fluorescence traces analyze well as the double exponentials predicted by Equation (20). The slower decays yield a rate constant of $(8.0 \pm 0.9) \times 10^5$ sec^{-1} $torr^{-1}$, equal to k_3 within experimental error. Thus the faster rise must give k_2, the rate of deactivation of $2\nu_2$. The data for the $2\nu_2$ rise times from these and Finzi's experiments are plotted in Figure 15. The slope gives $k_2 = (3.0 \pm 0.4) \times 10^6$ sec^{-1} $torr^{-1}$.

The total bending fluorescence, i.e., the sum of $2\nu_2$ and ν_2 fluorescence, is the sum of three exponentials as described by the sum of Equations (20) and (21). However, the experimental traces are well fit by double exponentials. Finzi's data gives a decay time of $(8.1 \pm 0.4) \times 10^5$ sec^{-1} $torr^{-1}$, in good agreement with the previously measured value of k_3. His data give a rate constant for the rise, denoted k_1', of $(2.0 \pm 0.2) \times 10^6$ sec^{-1} $torr^{-1}$, significantly smaller than k_2.

Two explanations for this must be considered. One is that the sum of the coefficients of the $\exp(-k_2[H_2O]t)$ terms in Equations (20) and (21), weighted by the appropriate radiative lifetimes, cancel. In this case k_1 would be given by the experimental k_1' with its error limits. Another possibility is that the rate constants k_1 and k_2 are close enough and the $\exp(-k_1[H_2O]t)$ and $\exp(-k_2[H_2O]t$ terms have amplitudes such that they combine to give an apparent single exponential over the 1 to 1.5 decades for which the fluorescence signal is larger than the noise.

To get limits on k_1 for the latter case an equation of the form

$$Q = D \exp(-k_2[H_2O]t) + E\exp(-k_1[H_2O]t)$$

was considered. The value of k_2 was fixed at 3×10^6 sec^{-1} $torr^{-1}$, D and E were allowed to vary arbitrarily, and Q was required to appear to be a single exponential of rate k_1' within the scatter of the data.

Figure 15. Inverse risetime vs pressure for $H_2{}^{18}O(2\nu_2)$ fluorescence experiments.

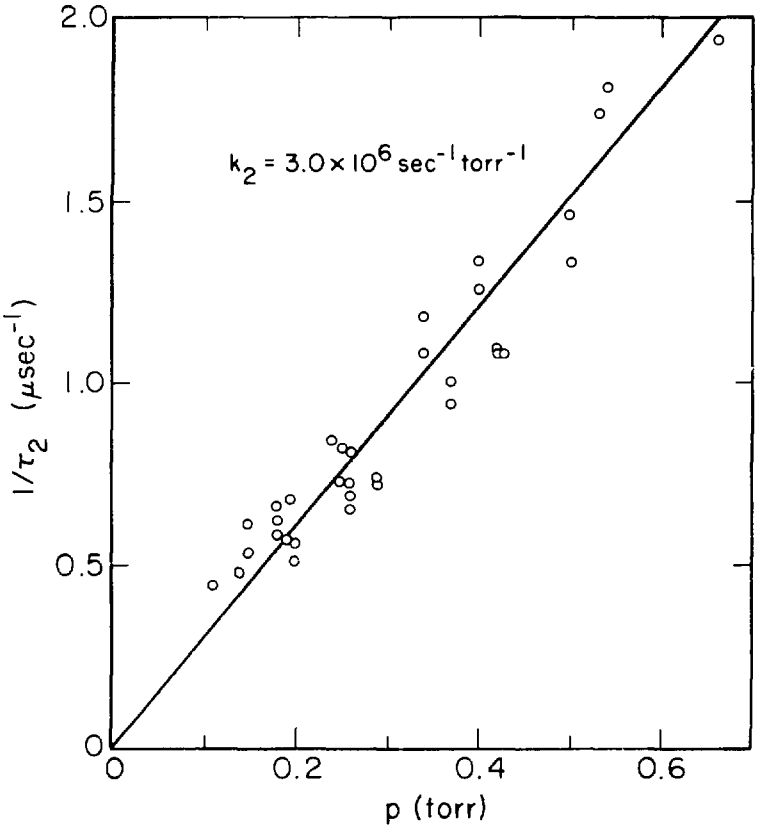

XBL 799-11661

Allowing all possible combinations of D and E gave 1.8×10^6 sec^{-1} $torr^{-1}$ $< k_1 < 3 \times 10^6$ sec^{-1} $torr^{-1}$. It should be noted that all values of k_1 between these limits could be made to fit the above requirements. For $k_1 < 1.8 \times 10^6$ sec^{-1} $torr^{-1}$ Q could no longer be made to appear to be a single exponential. The value of k_2 was chosen as an upper limit because k_2 is expected to be larger than k_1 due to contributions from the nearly resonant V→V channel and the expectation that $k'_{21} > k_{10}$. For HCl[40,41] and HF[42,43] 2→1 relaxation rates are much larger than 1→0 rates.

b. ν_1, ν_3 Quenching in Mixtures

Deactivation rates for the ν_1, ν_3 level by N_2, O_2, and CO_2 were determined. The contributions to the observed rate constant k_{obs} or observed lifetime τ_{obs} were calculated from

$$k_{obs} = 1/p\ \tau_{obs} = k_{H_2O}\ X_{H_2O} + k_M X_M, \tag{23}$$

where p is the total pressure, X_{H_2O} the mole fraction of water, X_M the mole fraction of the collision partner, k_{H_2O} the self-deactivation rate constant, and k_M the rate constant for deactivation by M. When $1/p\ \tau_{obs}$ vs X_{H_2O} is plotted for a series of measurements the intercept gives k_M and the slope gives $(k_{H_2O} - k_M)$.

Figures 16-18 give the results for N_2, O_2, and CO_2 respectively. The measured rate constants for ν_1, ν_3 deactivation by N_2 and O_2 are $(1.5 \pm 0.4) \times 10^4$ and $(1.1 \pm 0.4) \times 10^4$ sec^{-1} $torr^{-1}$, respectively. In addition the self-deactivation rate constant gotten from the slopes agrees with that from the pure water measurements within experimental error.

For CO_2 the deactivation rate constant is much faster, 1.1×10^5 sec^{-1} $torr^{-1}$. This is most likely due to the possibility of near-resonant V→V transfer to $CO_2(10^01)$, $CO_2(02^01)$, or perhaps $CO_2(00^01)$. However,

Figure 16. Plot of $1/p\tau$ vs $H_2{}^{18}O$ mole fraction for the $H_2{}^{18}O(\nu_3)$ fluorescence decays in N_2 mixtures.

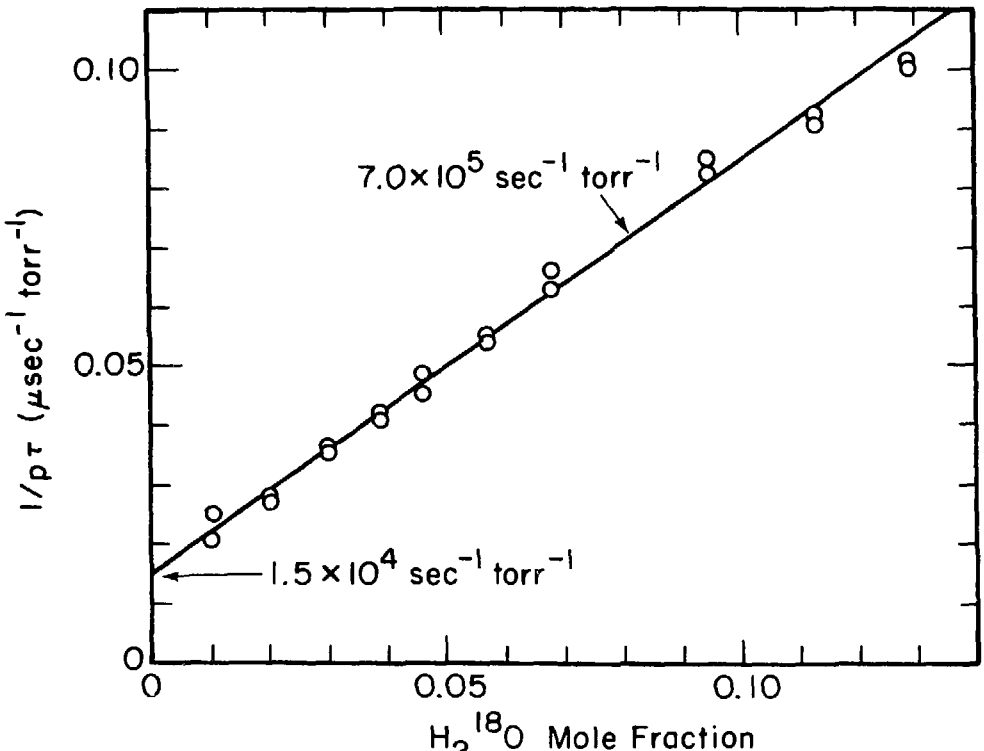

XBL 799-11663

Figure 17. Plot of $1/p\tau$ vs $H_2{}^{18}O$ mole fraction for the $H_2{}^{18}O(\nu_3)$ fluorescence in O_2 mixtures.

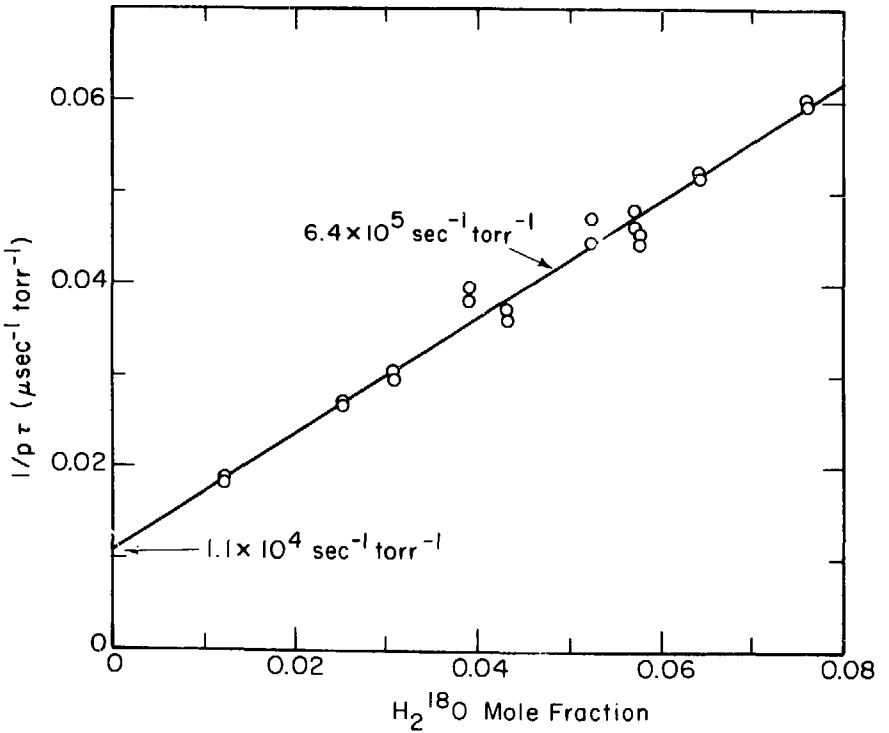

XBL 799-11664

Figure 18. Plot of $1/p\tau$ vs $H_2{}^{18}O$ mole fraction for the $H_2{}^{18}O(\nu_3)$ fluorescence in CO_2 mixtures. Slope = 0.55 μsec^{-1} $torr^{-1}$; intercept = 0.11 μsec^{-1} $torr^{-1}$.

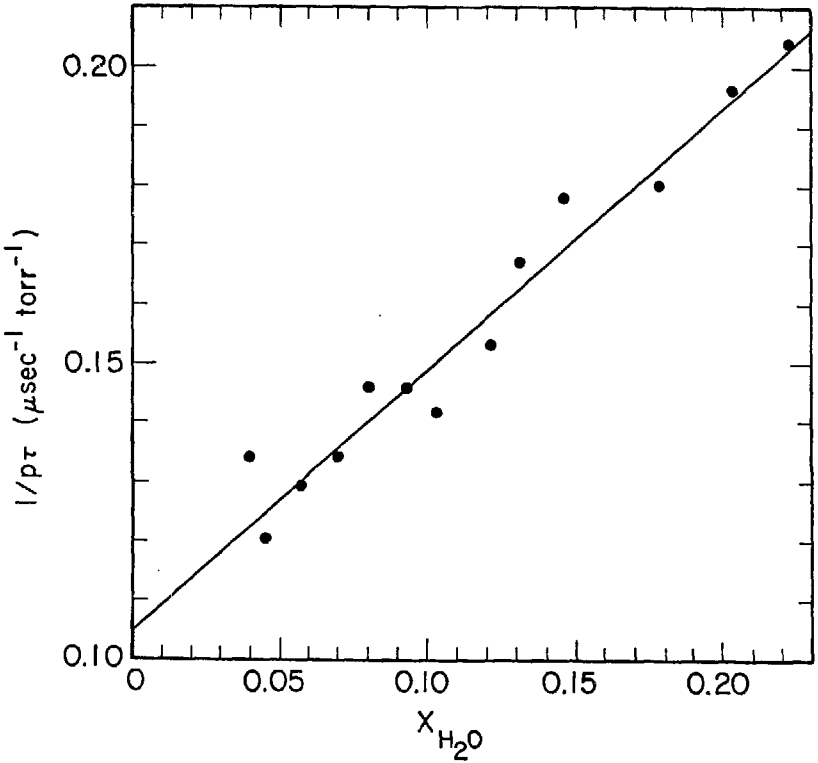

XBL 799-11665

the self-deactivation rate constant gotten from the slope, 5.4×10^5 sec^{-1} $torr^{-1}$, is low compared to the value from pure water. A model which allowed for reversible V→V transfer between the CO_2 and $H_2O(\nu_1, \nu_3)$ was tried using the known CO_2 self-quenching rates,[31] but this failed to account for the decreased slope. It should be noted that for all of these mixture experiments the cooled sidearm on the fluorescence cell contained frozen water. It is possible that when the CO_2 was added it formed a chemisorbed layer on the surface of the ice and lowered the H_2O partial pressure, thus decreasing the slope of the $1/p\tau$ vs X_{H_2O} plot. Whatever the effect, in the limit $X_{H_2O} \to 0$ the intercept will give k_{CO_2} so the value obtained from Figure 18 is certainly correct to within ±50%.

c. Relative Intensity Measurements

The ratio of the total number of photons emitted by $H_2O(\nu_2)$ to the total number emitted by $H_2O(2\nu_2)$, defined as F in Equation (22), was measured for pure $H_2{}^{18}O$. The $H_2O(\nu_2)$ area was taken as the difference between the observed total bending and bending overtone areas. F was found to be 0.84 ± 0.16, where the uncertainty is chosen to include the full range of experimental values measured at 0.086, 0.113, 0.144, and 0.179 torr. The primary source of the uncertainty in F is due to varying absorption and thus fluctuating fluorescence intensities. At too high a pressure self-absorption of the ν_2 fluorescence would cause an error in the measured F value. Finzi[31] found that the total bending fluorescence intensity increased linearly with pressure up to about 0.2 torr. This shows that below 0.2 torr self-absorption is not important.

Using Equation (22) we can write

$$\frac{2k_{21} + k'_{21}}{2k_2} + \frac{2k_{31} + k'_{31}}{2k_{32}} = \left(\frac{\tau_1}{2\tau_2}\right)\left(\frac{k_1}{k_2}\right) F. \tag{24}$$

For the radiative lifetime ratio we use the harmonic oscillator approximation $\tau_1 = 2\tau_2$. The maximum value of k_1/k_2 is unity and of the experimentally observed F is 1.0. Thus, the rhs of Equation (24) is clearly less than 1.0 and may be as small as 0.40. The lhs of Equation (24) consists of two important branching ratios for the energy flow. The first is the fraction of bending quanta transferred out of $2\nu_2$ which appear in ν_2. It is by definition less than one. The second is the branching ratio for the production of bending quanta in ν_2 vs $2\nu_2$ by deactivation of ν_1, ν_3. It is necessarily less than the rhs, which is in turn less than 1.0. Thus, we may deduce unambiguously that at least one-half of the bending quanta are initially produced in the $2\nu_2$ level.

Experiments give us no direct determination of the relative magnitudes of k_{21}, k'_{21}, or k_{20}. In most molecules we would safely assume that the V→V rate would be very much greater than the V→T,R rates and thus $k_{21} \gg k'_{21}$, k_{20}. For water it seems more likely that $k'_{21} > k_{21}$. This follows from the fact that the experimental value of k_{10} is at least half that of k_2. Even for water it seems safe to assume that the $2 \rightarrow 1$ V→T,R rate would be greater than the $1 \rightarrow 0$ rate, i.e., $k'_{21} \geq k_{10}$. With the large cross section, the V→V and the $2 \rightarrow 0$ V→T,R processes might take a bit away from the $2 \rightarrow 1$ cross section, but ordinarily we might expect $k'_{21} \approx 2k_{10}$. Thus, we presume $k'_{21} \geq k_{10} > 1.8 \times 10^6$ sec^{-1} $torr^{-1}$, and therefore $k'_{21} > \frac{1}{2} k_2$. This limits the first ratio on the lhs of Equation (24) to values between 1/4 and 3/4. The upper limit for the second ratio is then 3/4 and the lower limit remains zero. Thus, we may conclude that the dominant relaxation channel is transfer from the

stretching vibrations to the bending overtone vibration, followed by sequential V→T,R transfers of bending quanta.

C. Temperature Dependence of $H_2{}^{18}O$ ν_1, ν_3 and $2\nu_2$ Quenching

1. Experimental

For these studies a newer, higher energy Nd:YAG pumped OPO system was used. Because of the increased energy and bandwidth of the OPO output, scattered light was more of a problem, and it wasn't possible to extract rate constants from ν_3 fluorescence. However, by analyzing $2\nu_2$ emission as described previously, it was possible to measure both the ν_1, ν_3 and $2\nu_2$ quenching rate constants.

The Nd:YAG used to pump the OPO was a Raytheon model SS404 and provides up to 250 mJ/pulse TEM_{00} at a repetition rate of 10 Hz. The output has a pulse width of 10 nsec FWHM and a spectral bandwidth of 0.15 cm^{-1}. Typical Nd:YAG laser pumping energies ranged from 140 to 180 mJ/pulse.

The OPO is of the general design described by Brosnan and Byer.[44] For these experiments the total OPO output was 5-10 mJ/pulse, implying about 2-4 mJ/pulse at the 3839.8 cm^{-1} idler frequency used to pump $H_2{}^{18}O(\nu_3)$. This is the same strong transition used in the previously described room temperature measurements. The bandwidth of the idler is 0.15 cm^{-1} and the pulse duration 10 nsec FWHM. An etalon in the OPO cavity allows convenient fine tuning over a 1.5 cm^{-1} free spectral range.

The idler frequency was set approximately using a SPEX 3/4 m monochromator. A spectrophone cell containing 4 torr of $H_2{}^{18}O$ was used to tune the OPO into resonance with the ν_3 absorption line. The reflected OPO beam from the fluorescence cell was passed through the spectrophone cell, and then the OPO was fine tuned to give maximum acoustic signal.

For all data taking the total OPO output was used. To insure that the signal wasn't absorbed, a Ge flat that completely blocked the signal and partially transmitted the idler was placed in front of the spectrophone. The maximum acoustic signal occurred at the same frequency with and without the Ge flat.

Because of the higher OPO output within the bandwidth of the absorption it wasn't necessary to use the short multiple pass fluorescence employed in the room temperature measurements. This greatly simplified the hot cell design, which was essentially the same as that used for the NH_3 studies (see Fig. 2). The only difference was a reduction of the length to 4 cm.

For the low temperature measurements a Lauda K-4/R recirculating bath with isopropanol was used. For high temperatures an oil bath was heated using a 750 W heating coil and vibration isolated stirrer. Temperature control was provided by a Fernwall #17000-0 Thermoswitch.

Since the cell was 4 m from the OPO, lenses, 5 cm in diameter f/40 and f/20 of CaF_2, were used to give a beam diameter of 3 mm at the fluorescence viewing region. The same collection optics, ir detector and signal averaging system as that described previously were used. However, the wide pass filter was replaced by a long pass filter with a 2080 cm^{-1} cut on frequency.

The fluorescence cell plus the glass and Apiezon-N grease manifold to which it was connected could be pumped to 10^{-6} torr. There was no cooled sidearm on the fluorescence cell, and mixtures were prepared the same way as described for the NH_3 experiments. The gas purities were the same as given previously.

2. Results and Analysis

To extract deactivation rate constants from $2\nu_2$ fluorescence, the same method of analysis as that for the room temperature studies was used. All of the $2\nu_2$ fluorescence traces were found to analyze as a sum of single rising and falling exponentials. The 293°K studies of pure $H_2{}^{18}O$ showed that the rate constant derived from the rise is the $2\nu_2$ deactivation rate constant and that from the decay the ν_1, ν_3 deactivation rate constant.

To insure that the interpretation of the rise and fall was made correctly as the temperature was changed, measurements in pure water were made at 250 ± 3°K, 274 ± 3°K, 350 ± 3°K, and 400 ± 4°K. Decreasing the temperature below 293 K increased both the rise and fall rate constants, but they never came close in magnitude. Similarly, as the temperature was increased above 293°K, both the rise and fall decreased but never overlapped. Thus we can conclude that over the temperature range of 250 K to 400°K the rising exponential gives the $2\nu_2$ deactivation rate constant and the falling exponential gives the ν_1, ν_3 deactivation rate constant. The raw data is shown in Figures 19 and 20. The rate constants at each temperature are calculated by averaging the results of all samples at that temperature. The lines in Figures 19 and 20 are drawn such that their slopes give these average values and their intercepts are zero.

Once the pure water rate constants were determined it was possible to measure the temperature dependence of the He and Ar deactivation rate constants. In the previous room temperature studies,[31] where it was possible to observe both ν_3 and $2\nu_2$ fluorescence, it was shown that the deactivation of ν_1, ν_3 by Ar was significantly slower than deactivation of $2\nu_2$ by Ar. In this case, for any mixture of Ar and H_2O, the rise of

Figure 19. Temperature dependence of $H_2{}^{18}O(\nu_1,\nu_3)$ deactivation: ● - 250°K, slope = 1.4 μsec^{-1} $torr^{-1}$; + - 274°K, slope = 1.0 μsec^{-1} $torr^{-1}$; ▲ - 350°K, slope = 0.59 μsec^{-1} $torr^{-1}$; x - 400°K, slope = 0.48 μsec^{-1} $torr^{-1}$.

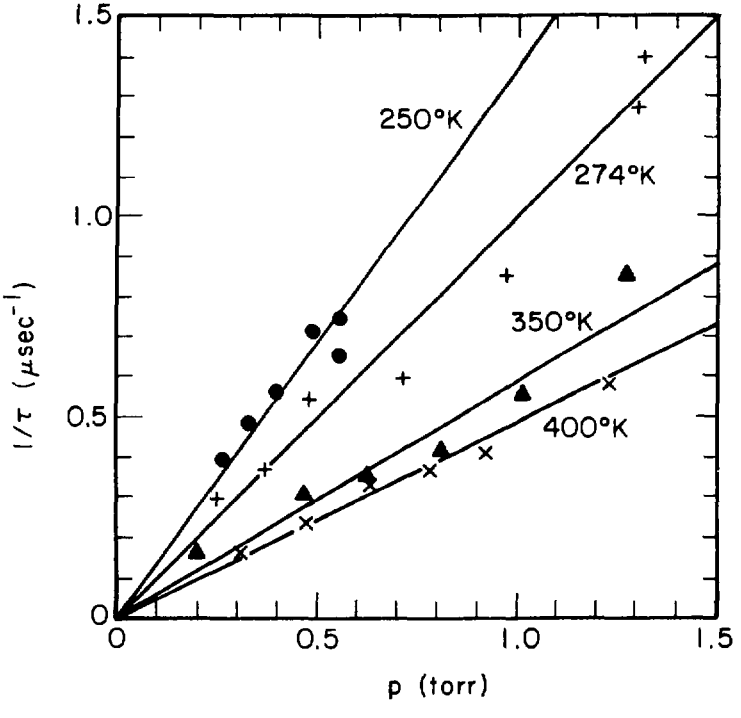

XBL 799-11666

Figure 20. Temperature dependence of $H_2{}^{18}O(2\nu_2)$ deactivation: ● - 250°K, slope = 4.5 μsec^{-1} $torr^{-1}$; + - 274°K, slope = 3.8 μsec^{-1} $torr^{-1}$; ▲ - 350°K, slope = 2.5 μsec^{-1} $torr^{-1}$; x - 400°K, slope = 1.9 μsec^{-1} $torr^{-1}$.

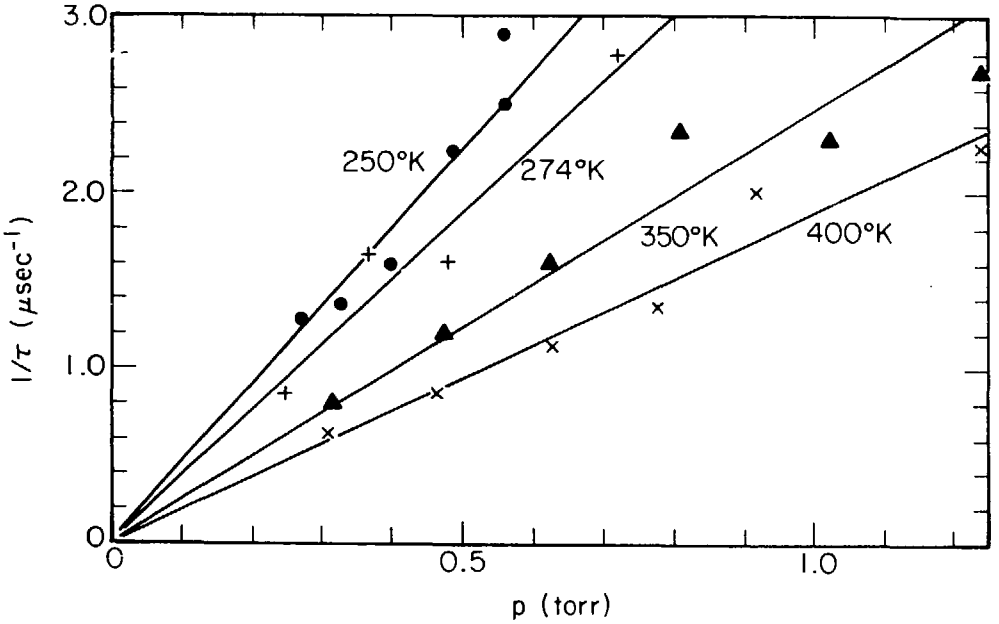

XBL 794-1166

the $2\nu_2$ fluorescence gives the sum of processes that deactivate $2\nu_2$ and the decay gives the sum of processes that deactivate ν_1, ν_3.

To determine the He and Ar deactivation rate constants the following procedure was used. First a few relaxation rates were measured in mixtures with mole fractions such that the relaxation was predominantly H_2O self-relaxation. As with pure H_2O the rise gives the $2\nu_2$ relaxation time and the fall the ν_1, ν_3 relaxation time. Then four to six measurements were made at low mole fractions and they were analyzed assuming the rise still gave $2\nu_2$ relaxation times and the fall gave ν_1, ν_3 relaxation times. Using all these points a $1/p\tau$ vs X_{H_2O} plot was made for both the rise and fall data. If the interpretations of the rise and fall were correct the plots should be linear with slopes giving the appropriate self-relaxation time. Figure 21 shows such a plot for the He data at 250°K. Clearly, the only consistent picture results from the interpretation used. If at the low X_{H_2O} points one reverses the interpretation of the rise and fall, the result is a ν_1, ν_3 self-relaxation rate constant that is a factor of 2 too slow and a negative rate constant for $2\nu_2$ relaxation by He. Such analyses for He or Ar at 250 ± 3°K, 296 ± 2°K, and 400 ± 4°K showed that for all X_{H_2O} the correct interpretation is to assign $2\nu_2$ relaxation to the rise and ν_1, ν_3 relaxation to the decay. The raw data is displayed in Figures 21-26. The reported buffer gas rate constants were calculated as in the NH_3 experiments, with only low X_{H_2O} points being used and corrections made for self-relaxation using the rate constants measured from pure water samples.

The uncertainties reported are calculated in two ways. For the self-relaxation rate constants the pressure was monitored continuously and changed <2% for all experiments. In this case the usual statistical

Figure 21. Results of analysis of $H_2{}^{18}O(2\nu_2)$ fluorescence in He mixtures at 250°K. + - from decay times, $k_{He} = 2.1 \times 10^{-3}$ μsec^{-1} $torr^{-1}$. ● - from rise times, $k_{He} = 7.4 \times 10^{-3}$ μsec^{-1} $torr^{-1}$.

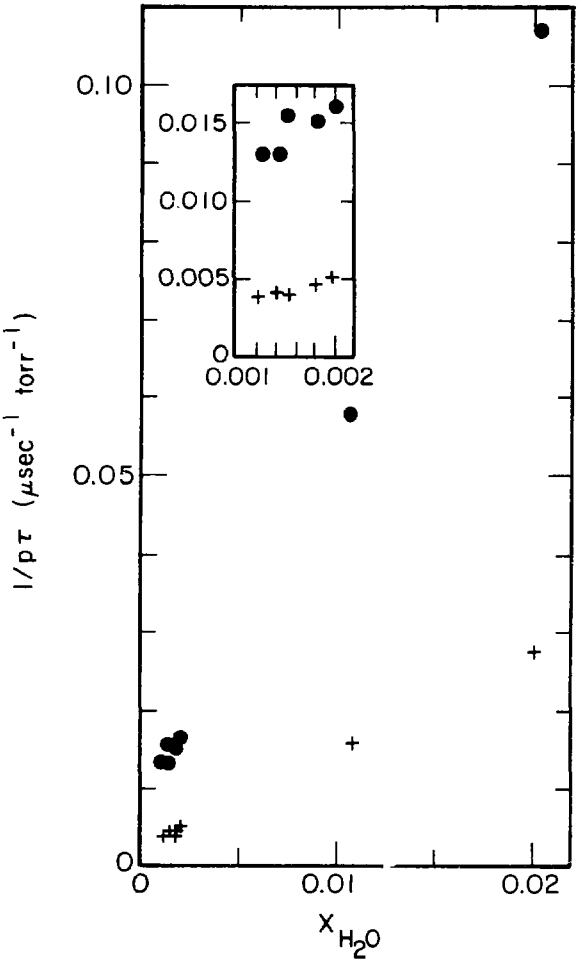

XBL 799-11668

Figure 22. Results of analysis of $H_2{}^{18}O(2\nu_2)$ fluorescence in Ar mixtures at 250°K. + - from decay times, $k_{Ar} = 1.1 \times 10^{-3}$ μsec^{-1} $torr^{-1}$. ● - from rise times, $k_{Ar} = 7.6 \times 10^{-3}$ μsec^{-1} $torr^{-1}$.

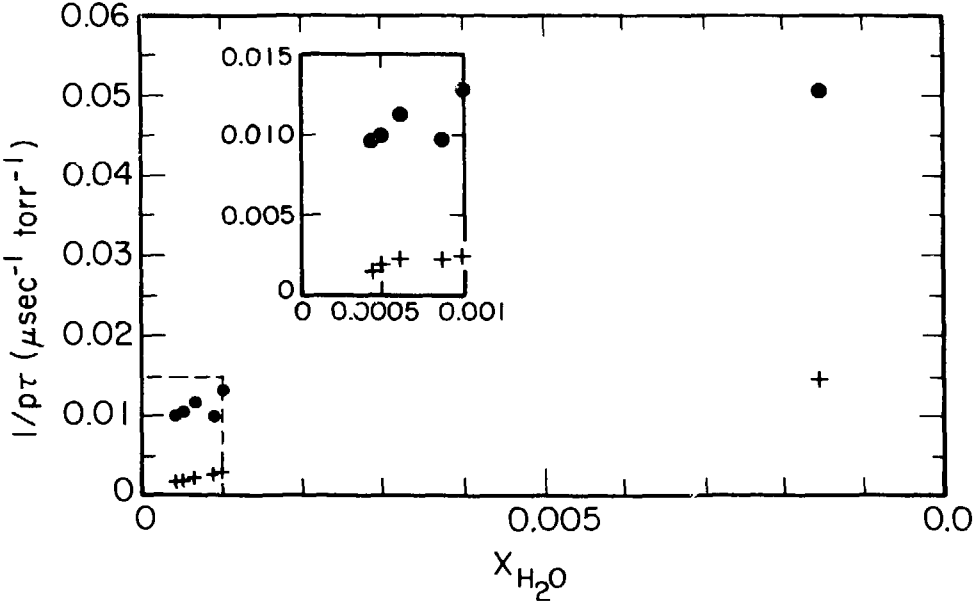

XBL 799-11669

Figure 23. Results of analysis of $H_2{}^{18}O(2\nu_2)$ fluorescence in He mixtures at 296 K. + - from decay times, $k_{He} = 2.1 \times 10^{-3}$ μsec^{-1} $torr^{-1}$. ● - from rise times, $k_{He} = 1.0 \times 10^{-2}$ μsec^{-1} $torr^{-1}$.

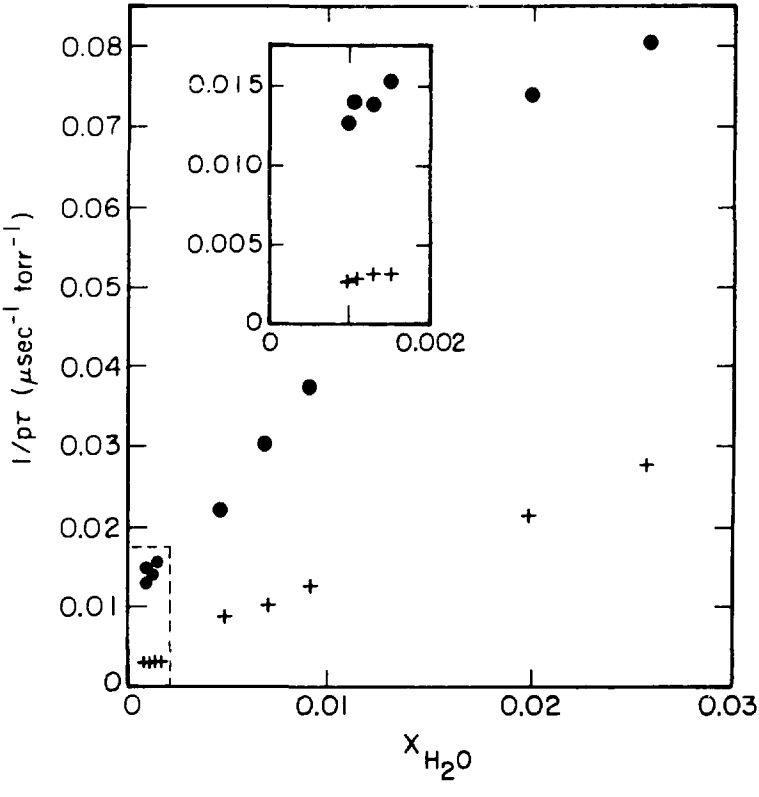

XBL 799-11670

Figure 24. Result of analysis of $H_2{}^{18}O(2_{12})$ fluorescence in Ar mixtures at 296 K. + - from decay times, $k_{Ar} = 2.0 \times 10^{-3}$ μsec^{-1} $torr^{-1}$. ● - from rise times, $k_{Ar} = 1.1 \times 10^{-2}$ μsec^{-1} $torr^{-1}$.

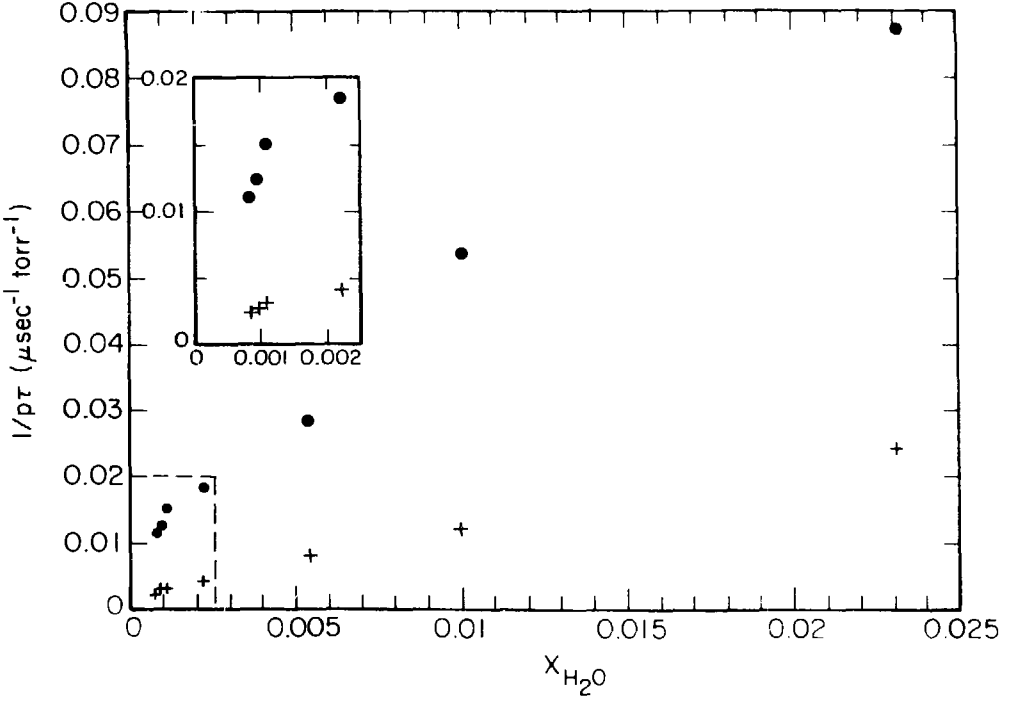
0.09
0.08
0.07
0.06
0.05
0.04
0.03
0.02
0.01
0
1/pτ (μsec⁻¹ torr⁻¹)
0
0.005
0.01
0.015
0.02
0.025
X H2O
0.02
0.01
0
0
0.001
0.002

Figure 2[illegible]. Results of analysis of $H_2{}^{18}O(2\,{}^1_2)$ fluorescence in He mixtures at 400°K. + - from decay times, $k_{He_2} = 1.8 \times 10^{-3}$ μsec^{-1} $torr^{-1}$. ● - from rise times, $k_{He} = 1.1 \times 10^{-2}$ μsec^{-1} $torr^{-1}$.

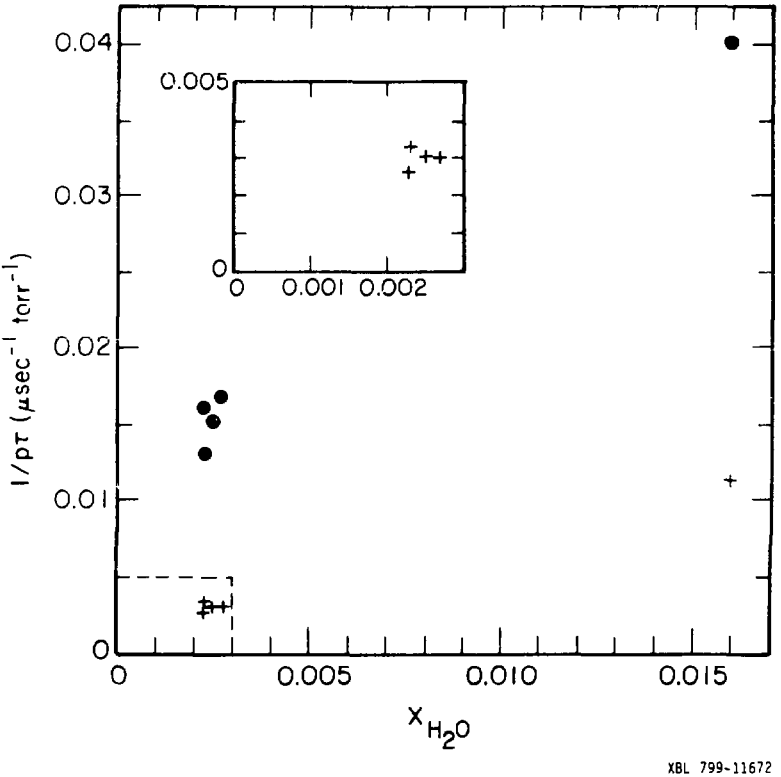

XBL 799-11672

Figure 26. Results of analysis of $H_2{}^{18}O(2\Sigma_2)$ fluorescence in Ar mixtures at 400°K. + - from decay times, $k_{Ar} = 1.7 \times 10^{-3}$ μsec^{-1} $torr^{-1}$. ● - from rise times, $k_{Ar} = 1.8 \times 10^{-2}$ μsec^{-1} $torr^{-1}$.

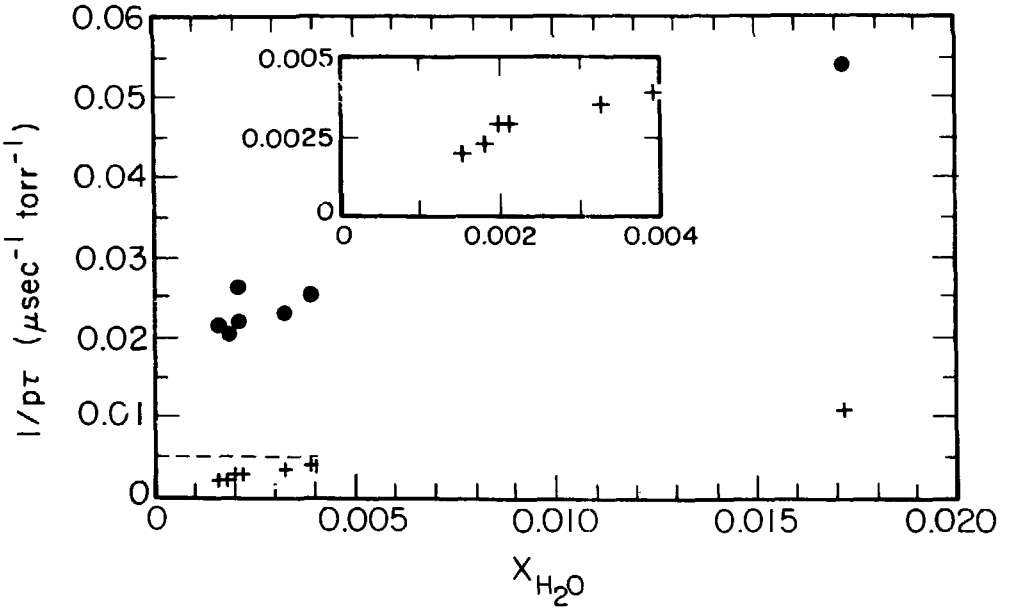

XBL 799-11673

analysis is appropriate and the uncertainties reported represent one standard deviation. The He and Ar measurements are subject to the same possible systematic errors described for the NH_3 measurements, and uncertainties were estimated in the same manner. In this case $\Delta(1/p\tau)$'s were estimated to be ±10% (a larger value than for NH_3 because of increased uncertainty in analyzing double exponentials) and the Δk_{H_2O}'s were the one standard deviation described above. The ΔX_{H_2O}'s were estimated to be ±10% by a comparison of the self-deactivation rate constants obtained from pure water samples to those obtained from mixtures. The average difference between the self-relaxation rate constants from pure water and those from the slopes of Figures 21-26 was found to be 10%.

A summary of the $H_2{}^{18}O$ deactivation rate constants and their uncertainties are given in Tables III and IV. The implications of these results will be taken up in the next chapter.

Table III

Deactivation of $H_2{}^{18}O(^1\Delta_1)$ by M

M	T(°K)	k(μsec^{-1} torr^{-1})	k(cm^3 molecule^{-1} sec^{-1})	$\bar{\sigma}(\text{Å})^a$	P^a
$H_2{}^{18}O$	250	1.4 ± 0.14	(3.5 ± 0.35) x 10^{-11}	4.9	0.20
	293	0.75 ± 0.7	(2.2 ± 0.2) x 10^{-11}	2.7	0.11
	400	0.48 ± 0.05	(2.0 ± 0.2) x 10^{-11}	2.2	0.088
He	250	(2.1 ± 0.8) x 10^{-3}	(5.4 ± 2.1) x 10^{-14}	4.4 x 10^{-3}	2.2 x 10^{-4}
	296	(2.1 ± 0.5) x 10^{-3}	(6.4 ± 1.5) x 10^{-14}	4.6 x 10^{-3}	2.3 x 10^{-4}
	400	(1.8 ± 0.5) x 10^{-3}	(7.3 ± 2.0) x 10^{-14}	4.6 x 10^{-3}	2.3 x 10^{-4}
Ar	250	(1.1 ± 0.4) x 10^{-3}	(2.8 ± 1.0) x 10^{-14}	4.5 x 10^{-3}	1.8 x 10^{-4}
	296[b]	(2.0 ± 0.5) x 10^{-3}	(6.2 ± 1.5) x 10^{-14}	8.8 x 10^{-3}	3.5 x 10^{-4}
	400	(1.7 ± 0.5) x 10^{-3}	(7.0 ± 2.0) x 10^{-14}	8.8 x 10^{-3}	3.5 x 10^{-4}
N_2	293	(1.5 ± 0.4) x 10^{-2}	(4.6 ± 1.2) x 10^{-13}	6.4 x 10^{-2}	2.3 x 10^{-3}
O_2	293	(1.1 ± 0.4) x 10^{-2}	(3.3 ± 1.2) x 10^{-13}	4.6 x 10^{-2}	1.8 x 10^{-3}
CO_2	293	0.11 ± 0.05	(3.3 ± 1.6) x 10^{-12}	0.35	1.0 x 10^{-2}

[a] Calculated using the molecular diameters d_{H_2O} = 2.8 Å, d_{He} = 2.24 Å, d_{Ar} = 2.86 Å, d_{N_2} = 3.15 Å, d_{O_2} = 2.93 Å, and d_{CO_2} = 3.92 Å. $\bar{\sigma} = k/\bar{v}$.

[b] This value is smaller than that reported in Reference 39, but these measurements were done under conditions where it could be more accurately measured.

Table IV

Deactivation of $H_2{}^{18}O(2_{12})$ by M

M	T(°K)	k(μsec^{-1} torr^{-1})	k(cm^3 molecule^{-1} sec^{-1})	$\bar{\sigma}$(Å^2)[a]	P[a]
$H_2{}^{18}O$	250	4.5 ± 0.4	(1.2 ± 0.1) x 10^{-10}	16	0.65
	293	3.0 ± 0.4	(9.1 ± 1.2) x 10^{-11}	12	0.47
	400	1.9 ± 0.2	(7.8 ± 0.8) x 10^{-11}	8.6	0.35
He	250	(7.4 ± 2.7) x 10^{-3}	(1.9 ± 0.7) x 10^{-13}	1.5 x 10^{-2}	7.6 x 10^{-4}
	296	(1.0 ± 0.2) x 10^{-2}	(3.2 ± 0.7) x 10^{-13}	2.2 x 10^{-2}	1.1 x 10^{-3}
	400	(1.1 ± 0.3) x 10^{-2}	(4.4 ± 1.0) x 10^{-13}	2.8 x 10^{-2}	1.4 x 10^{-3}
Ar	250	(7.6 ± 1.5) x 10^{-3}	(2.0 ± 0.4) x 10^{-13}	3.0 x 10^{-2}	1.2 x 10^{-3}
	296	(1.1 ± 0.2) x 10^{-2}	(3.2 ± 0.7) x 10^{-13}	4.8 x 10^{-2}	1.9 x 10^{-3}
	400	(1.8 ± 0.3) x 10^{-2}	(7.6 ± 1.4) x 10^{-13}	9.3 x 10^{-2}	3.7 x 10^{-3}

[a] Calculated using the molecular diameters d_{H_2O} = 2.8 Å, d_{He} = 2.24 Å, d_{Ar} = 2.86 Å. $\bar{\sigma} = k/\bar{v}$.

CHAPTER IV

DISCUSSION

A. Introduction

In this final chapter the implications of the measurements just described will be discussed. In Sections B and C comparisons will be made to other measurements of the same rates, to rates for similar systems, and to theoretical predictions. Next Section D will follow with an application of the temperature dependences observed to H_2O vapor laser optimization. In Section E we will show that a scheme for H_2O detection at high altitudes by looking at sunlight induced ir emission is feasible. Section F gives a brief discussion of the application of H_2O (ν_1, ν_3) quenching by CO_2 to understanding the ir emission from Mars and Venus. Section G summarizes this work and suggests areas of interest for further research.

B. Comparison to Other Measurements

Many attempts have been made to measure the relaxation rate of H_2O (ν_2) with acoustic techniques.[45,46] In pure water the vibrational relaxation is strongly masked by the much larger rotational relaxation and classical sound absorption. In measurements of a few percent of H_2O in O_2 the vibrational relaxation is moved to sufficiently low frequency and the vibrational heat capacity is sufficiently large (due to the O_2 which V→V exchanges rapidly with the H_2O) that moderately accurate measurements can be made. Bass and Shields[17] find energy transfer probabilities of 0.20 ± 0.05 in the temperature range 300-500°K. Their room temperature rate $k_{10} = 1.3 \pm 0.3\ \mu sec^{-1}\ torr^{-1}$ is not far from the lower limit established here. The many other data which have

gained considerable self-consistency over the years ($k_{10} \approx 0.15$ μsec^{-1} $torr^{-1}$)[45] are completely incompatible with the laser fluorescence results. Such slow decay rates would have been easily observable by laser fluorescence.

Kung and Center[47] have measured the relaxation of ν_2 by H_2O, He, Ar, and N_2 in a shock tube experiment covering the temperature range 1800-4100°K. Their experiment is not sensitive to the value of k_{32} and shows only that it is within an order of magnitude of k_{10}. The observed temperature independence of $p\tau$ would imply energy transfer probabilities proportional to $T^{\frac{1}{2}}$. This variation is, however, too small compared to experimental uncertainties to be significant. The observed probabilities at high temperature are essentially the same as found here for room temperature.

In a recent study of the quenching of Br(4 $^2P_{1/2}$) by H_2O Hariri and Wittig[48] used the resulting H_2O (ν_1, ν_3) fluorescence to measure the total self-quenching of H_2O (ν_1, ν_3). They report a value of 1.0 ± 0.3 μsec^{-1} $torr^{-1}$. In a similar study of the quenching of I(5 $^2P_{1/2}$) by H_2O, Grimley and Houston[49] find an H_2O (ν_1, ν_3) self-relaxation rate of 0.77 ± 0.09 μsec^{-1} $torr^{-1}$. Both of these results are at room temperature and compare with the value of (0.75 ± 0.07) μsec^{-1} $torr^{-1}$ obtained here. Thus all of the direct measures of H_2O (ν_1, ν_3) self-deactivation are in quite good agreement.

Most of the recent room temperature measurements of NH_3 (ν_2) self-relaxation by acoustic techniques are in reasonable agreement with that reported here, considering the difficulties of large corrections for classical absorption and rotational relaxation. Lambert and Salter[6] saw no sound velocity dispersion over the f/p range they studied and thus

concluded $k_{NH_3} > 1.1$ μsec^{-1} $torr^{-1}$. Cottrell and Matheson[7] did similar measurements and report similar results. Jones et al.[9] measure both velocity dispersion and absorption at larger f/p values. By fitting their results with the same relaxation time for both rotational and vibrational relaxation they obtain a value for k_{NH_3} of 1.8 μsec^{-1} $torr^{-1}$, but report no uncertainties. Of the recent measurements by acoustic techniques, the value of ~ 0.22 μsec^{-1} $torr^{-1}$ for k_{NH_3} by Strauch and Decius[8] from the velocity data is the furthest from that reported here.

Bass and Winter[10] measure k_{NH_3} from 300°K to 773°K. At 300°K they report a value of 0.73 μsec^{-1} $torr^{-1}$. However, their estimated uncertainties in this value due to a 10% uncertainty in the absorption measurements include values ranging from 0.45 μsec^{-1} $torr^{-1}$ to 1.8 μsec^{-1} $torr^{-1}$. They note that the difference between their result and that of Jones et al.[9] can be largely attributed to the different methods used to extract relaxation times from absorption data. Their values of k_{NH_3} decrease monotonically as T is increased to 0.45 μsec^{-1} $torr^{-1}$ at 773°K. Their uncertainties at 773°K include values from 0.35 to 0.6 μsec^{-1} $torr^{-1}$. Thus, although they report a probability of deactivation of 0.1 over the entire 300°K to 773°K range, their uncertainties include the values of Table II.

An infrared-ultraviolet double resonance technique used by Ambartzumian et al.[11] to study the room temperature V→T,R rate of NH_3 (ν_2) gave values of k_{Ar} and k_{O_2} of 7.0×10^{-3} μsec^{-1} $torr^{-1}$ and 1.1×10^{-2} μsec^{-1} $torr^{-1}$, in good agreement with those reported here. However, their value of k_{NH_3} was 0.69 ± 0.15 μsec^{-1} $torr^{-1}$, almost a factor of two slower than found here. An error in their NH_3 pressures could lead to a significant change in the k_{NH_3} value without significantly affecting the k_M's.

C. Comparison to Other Systems and to Theory

1. H_2O and NH_3 ν_2

A comparison of ν_2 V→T,R deactivation rates in the systems H_2O, D_2O, H_2S, D_2S, NH_3, and ND_3 illustrates the effects that hydrogen bonding and rotation have on vibrational relaxation. Table V gives the results of some experimental measurements of the rates for these systems. H_2O and NH_3 have strong hydrogen bonds of 3.5-5.6[53-58] and 2.8-4.5[58-61] kcal/mole, respectively, and deactivate quite rapidly. Even though deactivation of H_2O requires converting ~600 cm^{-1} more energy into translation and rotation, relaxation occurs more rapidly than for NH_3. This could be due in part to stronger hydrogen bonding. In addition, though, the rotational constants of H_2O are more than a factor of two larger than for NH_3. This could be important in enhancing V→R transfer.[62]

For H_2S, which interacts much less strongly than either H_2O or NH_3, the relaxation rates are more than an order of magnitude slower. The comparison between NH_3 and H_2S is especially useful because in this case the rotational constants are quite similar. It is thus clear that hydrogen bonding greatly enhances V→T,R relaxation.

A comparison of the hydride to deuteride relaxation rates in Table V indicates the importance of rotation in the relaxation process. In all cases the deuteride relaxes more slowly than the corresponding hydride. Such behavior has been observed for many hydride/deuteride systems[62] whether or not they are hydrogen bond. Using a modified SSH calculation in which the rotational velocity replaces the translational velocity Moore[62] is able to show the importance of V→R transfer for several systems. In this model it is their higher velocity of rotation that causes the hydrides to relax more rapidly. In addition, from this model one

Table V

Comparison of ν_2 V→T,R Relaxation for Some Polyatomic Hydrides and Deuterides at Room Temperature

Molecule	$k(\mu sec^{-1}\ torr^{-1})$	P^a	ν_2 frequency(cm^{-1})	Reference
$H_2{}^{18}O$	1.8 - 3.0	0.28-0.47	1588	This work
D_2O	1.0	0.16	1179	50, 51
NH_3	1.3	0.14	950	This work
ND_3	0.16	0.020	749	7
H_2S	0.048	0.0060	1290	52
D_2S	0.018	0.0023	934	51

[a] $P = k/k_{gk}$ and k_{gk} calculated using $d_{H_2O} = d_{D_2O} = 2.80$ Å, $d_{NH_3} = d_{ND_3} = 3.17$ Å, and $d_{H_2S} = d_{D_2S} = 3.59$ Å.

would expect that the relaxation rates increase with increasing temperature. This is seen to be the case for weakly interacting molecules such as CH_4.[63]

However, as is seen from the NH_3 data in Table II and the data on HCl[64] and HF,[65] the $J \rightarrow T,R$ relaxation rates of hydrogen bonding systems show negative temperature dependences near room temperature. In recent calculations on HF vibrational relaxation, to be discussed further in the next section, the importance of orbiting collisions in inducing vibrational energy transfer is shown.[66,67] The negative temperature dependence observed can be explained as being due to a decrease in the number of orbiting collisions as the average relative kinetic energy is increased. It is interesting to note that such orbiting collisions can be useful in explaining the relaxation properties of any system where the intermolecular attractions are larger than the average kinetic energy. Tusa et al.[68] recently studied the vibrational relaxation of I_2 in the v' = 14 level of the B state by He in a supersonic jet. The collision energies are low, only fluorescence from v' = 14 and v' = 13 could be observed, and the population in v' = 13 is larger than can be accounted for by a forced oscillator deactivation mechanism. They are able to fit their data by assuming that only very low energy collisions are involved, with the implication being that orbiting resonances or metastable complexes dominate the relaxation process.

The role of rotation is not as clear for relaxation processes in which such orbiting collisions occur. It is possible that the conversion of vibrational energy into rotation with the minimum possible ΔJ enhances the transfer probability. In this case, one would expect the hydrides to relax faster than deuterides. Whether this or some difference in the

collision dynamics causes the deuterides to relax more slowly isn't clear at this time.

Shin has investigated the V→T,R rates for NH_3 (ν_2) and H_2O (ν_2) using a V→T and a V→R model.[21] The V→T model assumes energy transfer occurs at preferred orientations. The importance of rotation discussed above indicates a V→T model is inappropriate, and the V→R model fails to predict the strong inverse temperature dependence we observe for NH_3.

In a recent calculation Shin[21] considers the relaxation of H_2O (ν_2) through formation of weakly bound complexes. His room temperature result is only about 30% slower than the lower limit established here, and he finds the expected negative temperature dependence. However, the average rotational period of a water molecule is at least a factor of two less than a typical nonorbiting collision time. The idea of a complex of defined geometry transferring energy into oscillatory modes seems unrepresentative of the collision dynamics involved.

2. H_2O (ν_1, ν_3) and H_2O ($2\nu_2$)

The stretch-to-bend V→V transfer probabilities may be compared to those for some other systems. For CH_4, Hess and Moore[69] find that $P_{CH_4-CH_4} \sim P_{CH_4-Ar}$. As seen from Table III we find $P_{H_2O-H_2O} >> P_{H_2O-Ar}$, illustrating the importance of hydrogen bonding in enhancing V→V as well as V→T,R rates. McGarvey et al.[70] have studied the deactivation of HCN (ν_3). They find the C-H stretch is coupled to the other modes with $P_{HCN-HCN} = 9 \times 10^{-3}$. The importance of hydrogen bonding is again illustrated by their result that $P_{HCN-Ar} \leq 10^{-5}$. The smaller probabilities compared to H_2O may result from the smaller rotational constants of HCN and the consequently increased difficulty of transferring the energy discrepancy into rotation. In light of this possibility it should be

noted that they also find that $P_{HCN-HF} = P_{HCN-DF}$ over the full 240°K - 450°K temperature range of their measurements. This indicates that it is the ability of the excited molecule to undergo efficient V→R transfer that is most important. Further evidence of the importance of rotation in the stretch-to-bend processes is seen in the results of Grimley and Houston. They find a room temperature probability for D_2O stretch deactivation that is a factor of 3 slower than that found for H_2O.

There are further similarities in the deactivation of H_2O and HCN stretches. HCN deactivation shows the same negative temperature dependence seen for H_2O. In addition, by also observing the decay of HCN (ν_2) fluorescence, McGarvey et al. conclude that the stretch-to-bend coupling is slower than the bend V→T,R rate, just as was seen for H_2O. This indicates that multiquantum V→V transfers are less efficient than V→T,R transfers of relatively large amounts of energy in these strongly interacting systems.

As was mentioned earlier, Poulsen et al.[66] and Billing and Poulsen[67] have calculated the V→V and V→T,R rates of energy transfer for HF from v = 1 to v = 7 over a wide temperature range. The calculation treated rotation and translation classically, explicitly accounted for orbiting collisions, and used an *ab initio* SCF HF-HF potential energy surface. Their findings are in qualitative agreement with a number of features observed in the H_2O system. For the temperature dependence of HF (v = 1) relaxation they find the experimentally observed negative temperature dependence near room temperature that goes through a minimum near 1000°K and then begins to increase. For H_2O, HCN, and NH_3 relaxation the negative temperature dependence has been observed but the measurements don't go to high enough temperatures to see where a minimum might occur. The

fact that Kung and Center[47] see a high temperature (1800°K - 4100°K) probability for H_2O (ν_2) deactivation close to the room temperature value shows that such a minimum most probably occurs.

As mentioned previously, the calculation shows the importance of orbiting collisions. They show that roughly half of the vibrational deactivation of HF (v = 1) at 300°K is a result of orbiting collisions. They also find orbiting collisions greatly enhance V→V transfer rates. Though orbiting collisions are shown to be important, the calculation plus experimental data indicate that the participation of long-lived collision complexes in which energy randomization occurs is not important. In the calculation, multiquantum transition probabilities were calculated for HF (v = 3) and found to be negligible. Douglas and Moore[71] have experimentally studied HF (v = 3, 4) relaxation. They find that within experimental error all of the HF (v = 4) deactivates to HF (v = 3). As discussed in Section III.B.3.c., H_2O (ν_1, ν_3) deactivates predominantly to H_2O ($2\nu_2$), showing that energy randomization has not occurred.

A final point of comparison is the relative magnitude of V→T,R and V→V rates. Billing and Poulsen[67] conclude that at 300°K HF (v = 2) deactivation is 42% V→T,R and for HF (v = 3) is 63% V→T,R. This is in spite of the large V→T,R energy discrepancies compared to V→V processes. Our observation that H_2O ($2\nu_2$) deactivates predominantly by a V→T,R process is in qualitative agreement with their conclusions for HF.

D. Effect of Rate Constants on Laser Operation.

As mentioned in Chapter I the temperature dependence of H_2O ν_1, ν_3 and $2\nu_2$ deactivation is important in determining the optimum operating conditions for the electric discharge pumped H_2O laser. The water vapor

laser oscillates on transitions from the stretching levels to the $2\nu_2$ level.[25] Sarjeant et al.[72] have measured relaxation times for the gain in an electrically excited H_2O laser. They report rate constants of 0.35 and 0.72 μsec^{-1} $torr^{-1}$ for transitions from ν_3 and ν_1, respectively. The temperature was thought to be 600°K. In a very rough approximation the rates correspond to k_3 (or perhaps to k_5 and k_4). Pichamuthu et al.[73] have observed the exponential decay time of a laser pulse, very roughly equal to the lower level decay time, and found a rate constant of 0.5 μsec^{-1} $torr^{-1}$, which should correspond to the k_2 observed here. Thus the effective rates measured in the laser media vary from equal to those in Tables III and IV to a factor of six slower. Better agreement cannot be expected in view of the complicated kinetics of the laser medium. The very fast relaxation rates require rapid excitation and relatively low operating pressures. A necessary condition for continuous laser action is that the relaxation of the lower level be rapid compared to that of the upper level. Thus, it is reassuring that k_2 is found to be greater than k_3. Since k_1 is also found to be greater than k_3, it may be possible to obtain laser action on transitions to the bending fundamental level.

There are several CW lines between ν_1 or ν_3 and $2\nu_2$ on which the laser will oscillate.[25] The problem of optimizing the CW laser transitions will be considered in terms of the model for a four level laser given by Yariv.[74] It is assumed that level 4 is pumped and couples rapidly to level 3, which would be the ν_1, ν_3 manifold. Oscillation occurs between level 3 and 2. The rate constants k_3 and k_2 represent the collisional deactivation of ν_1, ν_3 and $2\nu_2$, respectively. For simplicity it will be assumed that level 3 deactivates to level 2

exclusively. The spontaneous emission rates are much slower and can be ignored. The time dependence of levels 3 and 2 can then be written as

$$\frac{dN_3}{dt} = R_3 - k_3N_3N_1 - (N_3 - \frac{g_3}{g_2} N_2)\ W_{32}$$

$$\frac{dN_2}{dt} = R_2 + k_3N_3N_1 - k_2N_2N_1 + (N_3 - \frac{g_3}{g_2} N_2)\ W_{32}$$

where R_3 and R_2 are the pumping rates of levels 3 and 2 and $(N_3 - g_3/g_2\ N_2)\ W_{32}$ is the stimulated emission rate. In electric discharge lasers some pumping of level 2 is unavoidable. Assuming N_3, $N_2 << N_1$ and solving for steady-state conditions, i.e., $dN_3/dt = dN_2/dt = 0$ gives

$$\Delta N_{ss} \equiv (N_3 - \frac{g_3}{g_2} N_2)_{ss} = \frac{\left[R_3 - \frac{g_3k_3}{g_2k_2} (R_2 + R_3)\right]}{k_3N_T + W_{32}} \tag{25}$$

where N_1 has been replaced by N_T, the total H_2O number density. When ΔN_{ss} is below the threshold for oscillation, the cavity losses exceed the gain and there is zero oscillation energy density so that $W_{32} = 0$. When R_3 is increased to the point that the cavity losses equal the gain the threshold population inversion, ΔN_t, is reached. Increased pumping won't increase ΔN, but will result in $W_{32} > 0$ such that

$$\Delta N_t = R/(k_3N_T + W_{32}) \tag{26}$$

where $R = \left[R_3 - \frac{g_3k_3}{g_2k_2} (R_2 + R_3)\right]$ is the effective pumping rate. Thus for a given pumping rate such that ΔN_t is reached

$$W_{32} = R/\Delta N_t - k_3N_T. \tag{27}$$

The total power generated by stimulated emission, P_e, is given by

$$P_e = \Delta N_t V h\nu W_{32} = \Delta N_t V h\nu (R/\Delta N_t - k_3 N_T) \tag{28}$$

where V is the oscillating volume. The output power will be proportional to P_e, so optimizing P_e with respect to temperature will optimize the laser output.

In optimizing with respect to temperature the levels involved are sufficiently high that thermal populations can be ignored. From Tables III and IV it can be seen that k_3/k_2 is constant from 250°K to 400°K. The rates R_2 and R_3 are due either to direct electron impact or rapid cascading from higher levels.[72] Since in electric discharges the electron temperature is much higher than the heavy particle temperature[75] R_3 and R_2 may have only a weak dependence on the heavy particle temperature. Thus R probably has only a weak temperature dependence. The other temperature dependent term in Equation (28) is k_3, which Table III shows decreases monotonically from 250°K to 400°K. Based on the analysis so far, the H_2O laser will be most efficient at elevated temperatures.

Account should also be taken of the effect that temperature has on the gain due to changes in linewidth and rotational distribution. To a reasonable approximation, the gain γ is inversely proportional to the linewidth. Assuming that the linewidth is primarily due to Doppler broadening, then $\gamma \propto T^{-\frac{1}{2}}$ and we have for the change in gain due to change in linewidth

$$\gamma(T_2) = \left(\frac{T_1}{T_2}\right)^{\frac{1}{2}} \gamma(T_1). \tag{29}$$

To estimate the effect on the gain due to changing the rotational distribution as the temperature increases it will be assumed that only

the stretching levels are pumped by the electric discharge. For this case $\gamma(T) \propto \Delta N_i(T)$, where $N_i(T)$ is the population of the initial rotational level in ν_1, ν_3. Assuming a Boltzman distribution of rotational states and using the classical expression for the rotational partition function, the change in gain due to changing population of the initial rotational state can be written as

$$\gamma(T_2) = \left\{\left(\frac{T_1}{T_2}\right)^{3/2} \exp\left[\frac{h\nu_i(T_2-T_1)}{kT_1T_2}\right]\right\}\gamma(T_1) \tag{30}$$

where $h\nu_i$ is the rotational energy of the initial state. For the CW lines of interest, most of the ν_i's are between 600 cm^{-1} and 1000 cm^{-1}.

The combined effect due to linewidth and rotational population effects is just the product of the two effects. Combining Equations (29) and (30) gives

$$\gamma(T_2) = G(T_2,T_1)\gamma(T_1) = \left\{\left(\frac{T_1}{T_2}\right)^{2} \exp\left[\frac{h\nu_i(T_2-T_1)}{kT_1T_2}\right]\right\}\gamma(T_1). \tag{31}$$

To see the effect, T_1 = 300°K and ν_i = 800 cm^{-1} were used to calculate the values of $G(T_2,T_1)$ for T_2 equal to 400°K, 600°K, 800°K, and 1000°K. The values are 1.5, 1.7, 1.6, and 1.3, respectively. It can thus be concluded that the optimum operating temperature would still be at elevated temperatures, with the exact temperature depending on how far beyond 400°K k_3 continues to decrease.

A similar analysis should apply to the two-photon pumped NH_3 laser that oscillates between $2\nu_2(-)$ and $1\nu_2(+)$.[26] In this case only k_2 has been measured. From Table II it is seen to be fast and inversely proportional to temperature. However, by comparison to H_2O $2\nu_2$ and ν_2 results one would expect k_3 for this laser to be faster than k_2 and to

also show a negative temperature dependence. Again, elevated temperatures would be expected to be more efficient, though thermal populations may cause the maximum to be reached at a lower temperature.

E. Analysis of H_2O Detection Scheme

It has been suggested that accurate water vapor concentration profiles in the upper stratosphere and mesophere might be deduced from sunlight-induced emission at the 2.7 μm ν_3 wavelength.[27] This section will consider the feasibility of such a scheme. The important parameter to estimate is the steady-state population of ν_3 due to pumping by absorption of sunlight and loss through collisions and spontaneous emission. Letting N_3 be the population of ν_3 we can write

$$\frac{dN_3}{dt} = R - k_3 \quad N_3 N_{H_2O} - \frac{N_3}{\tau_3} - \sum_M k_3^M N_3 N_M$$

where R is the pumping rate, k_3 the ν_3 self-deactivation rate constant, N_{H_2O} the H_2O number density, τ_3 the ν_3 radiative lifetime, k_3^M the deactivation rate constant by M, and N_M the total number density of M. N_2 and O_2 are by far the main atmospheric constituents and at 296°K deactivate ν_3 at nearly the same rate. The term $\sum_M k_3^M N_M$ will be replaced by simply $k_3^M N_M$ where $k_3^M = (k_3^{O_2} + k_3^{N_2})/2$ and $N_M = N_{O_2} + N_{N_2}$. At steady-state

$$N_3^{SS} = R/(k_3 N_{H_2O} + k_3^M N_M + 1/\tau_3). \tag{32}$$

To evaluate this, R must be estimated. This first requires estimating the solar intensity as a function of altitude. The range of interest is 40 km to 80 km. From 80 km outward the H_2O concentration is small enough that no significant absorption loss occurs. Using the data

[illegible] the average H_2O concentration in the 40 km to 80 km range [illegible] characterized as a function of altitude X by

$$N_{H_2O}(X) = \exp\left[(9/6 \times 10^{-6})(8 \times 10^{6} - X) + 20\right]. \tag{33}$$

where X is in cm and N_{H_2O} in molecules/cm^3. The solar flux intensity at a frequency ν with absorption cross section $\sigma(\nu)$ can be obtained by evaluating

$$I(X,\nu) = I_0(\nu) \exp\left[-\sigma(\nu) \int_{X'=8\times10^6}^{X} N_{H_2O}(X)\, dx\right]$$

$$= I_0(\nu) \exp\left[-\left(\frac{6}{9} \times 10^{-6}\right)\sigma(\nu)\left(e^{\left[\left(\frac{9}{6} \times 10^{-6}\right)(8 \times 10^{6} - X) + 20\right]} - e^{20}\right)\right] \tag{34}$$

where I is in (photons cm^{-2} sec^{-1}/cm^{-1}), $\sigma(\nu)$ in cm^2, and I_0 is the flux at 80 km. The rate that molecules are pumped at a given frequency and altitude becomes

$$R(X,\nu) = \frac{dI(X,\nu)}{dX} = \sigma(\nu) N_{H_2O}(X) I(X,\nu). \tag{35}$$

To find the pumping rate for a specific vibration-rotation transition i one should put in the appropriate lineshape for $\sigma_i(\nu)$ and integrate (35) from $\nu = 0$ to $\nu = \infty$. To avoid this we note that[77]

$$S_i = \int_0^\infty N\sigma_i(\nu)\, d\nu = S_i^\circ N \tag{36}$$

where S_i° is a constant called the line strength and N the number density of absorber. A reasonable approximation that avoids integrating (35) is to replace $\sigma_i(\nu)$ by a constant value σ_i such that

$$S_i^\circ = \sigma_i \Delta\nu \tag{37}$$

where $\Delta\nu$ is the appropriate linewidth. For H_2O (ν_3) transitions at the pressures of interest (<2 torr) the Doppler width of 0.01 cm^{-1} (FWHM) should be used. The pumping rate for a specific vibration-rotation transition R_i can then be written as

$$R_i(X) = R(X, \nu_i)\Delta\nu = \sigma_i N_{H_2O}(X) I(X, \nu_i)\Delta\nu \qquad (38)$$

Using (38) R_i was calculated for a strong, medium, and weak ν_3 transition with cross sections obtained from the data of Gates et al.[78] It should be noted that S_i° and thus σ_i are temperature dependent. The temperatures range from 180°K at 80 km to 250°K at 60 km to 270°K at 40 km.[76] A constant temperature of 230°K, roughly the median, was used to do the calculations. The R_i's at 40, 60, and 80 km are given for the three transitions in Table VI.

Finally, N_3^{ss} can be estimated using (32). onsider the case of 60 km where T ~ 250°K, N_{H_2O} ~ 10^{10} molecules/cm^3, and $N_{O_2} + N_{N_2}$ = 7.2 x 10^{15} molecules/cm^3. From Table III, $k_3^{H_2O}$ = 3.5 x 10^{-11} cm^3/molecule sec and a reasonable estimate of k_3^M is 3.5 x 10^{-13} cm^3/molecule sec. Using the fastest pumping rate from Table VI of 10^5 molecules/cm^3/sec and τ_3 = 14 msec gives N_3^{ss} ~ 40 molecules/cm^3. It should be noted that the dominant deactivation term is for collisions with O_2 and N_2. Looking at a 10 cm^{-1} bandwidth around the strong transition includes the medium line plus two slightly weaker lines and several weak lines. Assuming that this is the observed bandwidth then a reasonable estimate of the number of observable excited molecules is N_3^{ss} ~ 100 molecules/cm^3.

The question now becomes can this number density of excited molecules be observed? First we must consider how many photons can be collected by a detector of area A looking out into a cone of angle θ. For a

Table VI

$H_2O(\nu_3)$ Pumping Rates as a Function of Altitude and Cross-Section

σ_i (m^2)[a]	X(m)	N_{H_2O}(molecules/cm^3)	$I(X, \nu_i)$	$R_i(X)$ ($\frac{molecules}{cm^3\ sec}$)[e]
3.3×10^{-17}[b]	40	2.0×10^{11}	$0.014\ I_0$	4.0×10^4
	60	9.7×10^9	$0.82\ I_0$	1.1×10^5
	80	4.9×10^8	I_0	6.9×10^3
1.0×10^{-17}[c]	40	2.0×10^{11}	$0.27\ I_0$	2.3×10^5
	60	9.7×10^9	$0.94\ I_0$	3.9×10^4
	80	4.9×10^8	I_0	2.1×10^3
0.18×10^{-17}[d]	40	2.0×10^{11}	$0.79\ I_0$	1.2×10^5
	60	9.7×10^9	$0.99\ I_0$	7.4×10^3
	80	4.9×10^8	I_0	0.38×10^3

[a]Based on $\Delta\nu_D = 0.01\ cm^{-1}$, $T = 230°K$.

[b]$4_{04} - 3_{03}$ transition with $\nu_i = 3838\ cm^{-1}$.

[c]$4_{14} - 3_{13}$ transition with $\nu_i = 3835\ cm^{-1}$.

[d]$4_{32} - 3_{31}$ transition with $\nu_i = 3840\ cm^{-1}$.

[e]Based on $I_0 = 6.3 \times 10^{16}$ photons $cm^{-2}\ sec^{-1}\ \mu m^{-1}$ from Reference 79.

single molecule a distance h from the detector where h >> detector dimensions then F, the fraction of photons emitted that hit the detector is

$$F \sim A/4\pi h^2.$$

Now consider a spherical shell of thickness dh that is subtended by the cone of base angle θ. The number of emitters N_E in the shell is simply the volume of the shell times the number density of emitters or

$$N_E = N_3^{SS}\, 2\pi h^2 (1-\cos(\tfrac{\theta}{2}))dh.$$

The total number of photons per second from the cone of height H and angle θ then becomes

$$J_H = \frac{1}{\tau_3}\int_0^H FN_E = \frac{N_3^{SS} AH}{2\tau_3}(1-\cos(\tfrac{\theta}{2})) \tag{39}$$

where τ is the radiative lifetime.

The final question is whether J_H can be detected. From Hudson[80] the normalized detectivity D^* for a detector is related to the signal-to-noise S/N, detector area A, electrical bandwidth Δf, and power falling on the detector P by

$$D^* = \frac{S/N}{P}(A\Delta f)^{\frac{1}{2}} \tag{40}$$

Using (39) and (40) the photon flux from the cone will give

$$(S/N)_H = PD^*/(A\Delta f)^{\frac{1}{2}} = h\nu J_H D^*/(A\Delta f)^{\frac{1}{2}}$$

$$= \frac{h\nu D^* N_3^{SS} H}{2\tau_3}\left(\frac{A}{\Delta f}\right)^{\frac{1}{2}}(1-\cos(\tfrac{\theta}{2})). \tag{41}$$

Using data from Santa Barbara Research Center[81] a PbS detector of area 0.16 cm^2 with $D^* \sim 6 \times 10^{11}$ $cm(Hz)^{1/2}$/watt (2π steradian field-of-view, 295 K background) is a good choice. Assuming a detector (at an altitude of 60 km) looks parallel to the earth's surface into a cone of H = 10 km and $\theta = 30°$ the altitudes observed range from 57 km to 63 km. The PbS detector has its maximum D* at about 100 Hz. By chopping the signal at this rate and using phase sensitive detection the effective Δf can be reduced to 1 Hz. Using the average N_3^{ss} as the 100/cm^3 value estimated for 60 km, τ_3 = 14 msec, and ν = 3838 cm^{-1} gives a $(S/N)_{H=10} \sim 20$. This value could be improved upon by decreasing the noise field-of-view (2π steradian black body was assumed) and using cooled narrow band filters to increase the D*. The actual background should be significantly less than a 295°K black body. Thus it seems that the H_2O detection scheme is feasible.

F. Implications for Planetary Atmosphere Studies

The vibrational energy transfer rate from H_2O (ν_1, ν_3) to $CO_2(10^01)$ or $CO_2(02^01)$ is of interest to astronomers studying ir emission from the atmospheres of Mars and Venus. Johnson et al.[82] have reported observing strong 10 μm emission from the atmospheres of both of those planets due to non-thermal population of $CO_2(00^01)$. They propose two possible mechanisms to account for this. One involves direct absorption of the near ir solar flux by CO_2 followed by energy transfers to $CO_2(00^01)$. The other involves absorption of the near ir solar flux by H_2O followed by energy transfer to CO_2. For this second mechanism to contribute significantly they estimate that a transfer efficiency from H_2O to $CO_2(00^01)$ near unity is required. Since the total cross section for quenching of $H_2O(\nu_1, \nu_3)$ by CO_2 is two orders of magnitude less (Table

III), the second mechanism described above cannot contribute significantly to the non-thermal $CO_2(00^01)$ population.

6. Conclusions

The V→V and V→T,R relaxation rates of low lying vibrational levels of NH_3 and $H_2{}^{18}O$ have been found to be quite fast. The probabilities for self-relaxation at room temperature are all greater than 0.1. Tables II-IV summarize the quenching rates that were measured. Comparisons to experimental and theoretical studies of other strongly interacting systems revealed certain common features. The rates all show negative temperature dependences near room temperature. Deuterides deactivate more slowly than hydrides, indicating that rotation plays an important role in the vibrational relaxation. Multiquantum V→V transfers are slower than V→T,R transfers, even though the energy discrepancy is much larger for the V→T,R processes. Orbiting collisions seem to be quite important in causing the rapid relaxation rates.

Further studies are needed to fully understand the processes involved. Measurements at higher temperatures would show whether the expected minima in the relaxation rates occur. It would be interesting to know if the stretch-to-bend coupling in NH_3 is slower than the bend V→T,R rate, as was seen for H_2O and HCN. Experimental and theoretical studies of the rotational state-to-rotational state rates could give a better understanding of the role that rotation plays in the relaxation rates. These are also the most difficult studies. Through them one could hope to begin to make useful predictions for the relaxation rates over a wide variety of conditions.

REFERENCES

1. J. J. Hinchen, J. Chem. Phys. 59, 233 (1973).

2. J. L. Ahl and T. A. Cool, J. Chem. Phys. 58, 5540 (1973).

3. H.-L. Chen and C. B. Moore, J. Chem. Phys. 54, 4072 (1971).

4. J. T. Yardley and C. B. Moore, J. Chem. Phys. 49, 1111 (1968).

5. R. Klein and P. Hess, Acustica 33, 198 (1975).

6. J. D. Lambert and R. Salter, Proc. R. Soc. Sec. A 253, 277 (1959).

7. T. L. Cottrell and A. J. Matheson, Trans. Faraday Soc. 59, 824 (1963).

8. J. G. Strauch, Jr., and J. C. Decius, J. Chem. Phys. 44, 3319 (1966).

9. D. G. Jones, J. D. Lambert, M. P. Saksena, and J. L. Stretton, Trans. Faraday Soc. 65, 965 (1969).

10. H. E. Bass and T. G. Winter, J. Chem. Phys. 56, 3619 (1972).

11. R. V. Ambartzumian, V. S. Letokhov, G. N. Makarov, and A. A. Puretskii, Zh. Eksp. Teor. Fiz. 68, 1736 (1975); [Sov. Phys. - JETP 41, 871 (1976)

12. H.-J. Bauer, J. Acoust. Soc. Am. 44, 285 (1968).

13. A. A. Monkewicz, J. Acoust. Soc. Am. 42, 258 (1967).

14. M. C. Henderson, A. V. Clark, and P. R. Lintz, J. Acoust. Soc. Am. 37, 457 (1965).

15. M. C. Henderson and K. F. Herzfeld, J. Acoust. Soc. Am. 37, 986 (1965).

16. C. S. Tuesday and M. Boudart, Princeton University Technical Note 7, Contract AF 33 (038)-23976 (January 1955).

17. H. E. Bass and F. D. Shields, J. Acoust. Soc. Am. 56, 856 (1974).

18. Y. Fujii, R. B. Lindsay, and K. Urushihara, J. Acoust. Soc. Am. 35, 961 (1963).

19. H. Roesler and K.-F. Sahm, J. Acoust. Soc. Am. 37, 386 (1965).

20. H. E. Bass, J. R. Olson, and R. C. Amme, J. Acoust. Soc. Am. 56, 1455 (1974).

21. H. K. Shin, J. Am. Chem. Soc. 90, 3029 (1968); J. Phys. Chem. 77, 346 (1973); and J. Chem. Phys. 69, 1240 (1978).

22. B. Hartman and B. Kleman, Appl. Phys. Lett. 12, 168 (1968).

23. W. S. Benedict, Appl. Phys. Lett. 12, 170 (1968).

24. M. A. Pollack and W. J. Tomlinson, Appl. Phys. Lett. 12, 173 (1968).

25. W. S. Benedict, M. A. Pollack, and W. J. Tomlinson, IEEE J. Quantum Electron. 5, 108 (1969).

26. R. E. Jacobs, D. Prosnitz, W. R. Bischel, and C. K. Rhodes, Appl. Phys. Lett. 29, 710 (1976).

27. J. R. Drummond, 1978 (private communication).

28. T. Y. Chang and J. D. McGee, Appl. Phys. Lett. 28, 526 (1976).

29. F. Shimizu, J. Chem. Phys. 52, 3572 (1970).

30. J. S. Garing, H. H. Nielsen, and K. N. Rao, J. Mol. Spectrosc. 3, 496 (1959).

31. J. Finzi, Thesis, University of California, Berkeley (1979).

32. G. Herzberg, "Molecular Spectra and Molecular Structure II. Infrared and Raman Spectra of Polyatomic Molecules." (Van Nostrand Reinhold, New York, 1945), pp. 294-7.

33. C. H. Townes and A. L. Schalow, "Microwave Spectroscopy," (Dover Publications, Inc., New York, 1975), p. 342.

34. P. F. Zittel and C. B. Moore, J. Chem. Phys. 58, 2004 (1973).

35. P. E. Fraley, K. N. Rao, and L. H. Jones, J. Mol. Spectrosc. 29, 312 (1969).

36. P. E. Fraley and K. N. Rao, J. Mol. Spectrosc. 29, 348 (1969).

37. J. M. Flaud and C. Camy-Peyret, J. Mol. Spectrosc. 55, 278 (1975).

38. Y. B. Aryeh, J. Quant. Spectrosc. Radiat. Transfer 7, 211 (1967).

39. J. Finzi, F. E. Hovis, V. N. Panfilov, P. Hess, and C. B. Moore, J. Chem. Phys. 67, 4053 (1977).

40. S. R. Leone and C. B. Moore, J. Chem. Phys. 19, 340 (1973).

41. H.-L. Chen and C. B. Moore, J. Chem. Phys. 54, 4072 (1971).

42. N. Cohen and J. F. Bott, Appl. Opt. 15, 28 (1976).

43. J. F. Bott, J. Chem. Phys. 61, 3414 (1974).

44. S. J. Brosnan and R. L. Byer, IEEE J. Quantum Electron. QE-15, 415 (1979).

45 R. G. Keeton and H. E. Bass, J. Acoust. Soc. Am. 60, 78 (1976).

46. R. L. Taylor and S. Bitterman, Rev. Mod. Phys. 41, 26 (1969).

47. R. T. V. Kung and R. E. Center, J. Chem. Phys. 62, 2187 (1975).

48. A. Hariri and C. Wittig, J. Chem. Phys. 68, 2109 (1978).

49. A. J. Grimley and P. L. Houston, J. Chem. Phys. 69, 2339 (1978).

50. R. L. Sheffield, K. Boyer, and A. Javan, private communication (1979).

51. S. Miljanic and C. B. Moore, private communication (1979).

52. H.-J. Bauer, A. C. C. Paphitis, and K. Schotter, Physica 47, 109 (1970).

53. W. P. Luck, in "The Hydrogen Bond, Recent Developments in Theory and Experiments", edited by P. Schuster, G. Zundel, and C. Sandorry (North-Holland, New York, 1976) p. 1396.

54. H. A. Gebbie, W. J. Burroughs, J. Chamberlain, J. E. Harries, and R. G. Jones, Nature, 221, 143 (1969).

55. C. Braun and H. Leidecker, J. Chem. Phys. 61, 3104 (1974).

56. L. L. Shipman and H. A. Scheraga, J. Phys. Chem. 78, 909 (1974).

57. G. H. F. Diercksen, W. P. Kraemer, and B. O. Roos, Theor. Chim. Acta, 36, 249 (1975).

58. J. D. Dill, L. C. Allen, W. C. Topp, and J. A. Pople, J. Am. Chem. Soc. 97, 7220 (1975).

59. J. S. Rowlinson, Trans. Faraday Soc. 45, 974 (1949).

60. J. D. Lambert, Discuss. Faraday Soc. 15, 226 (1953).

61. J. E. Lowder, J. Quant. Spectrosc. Radiat. Transfer, 10, 1085 (1970).

62. C. B. Moore, J. Chem. Phys. 43, 2979 (1965).

63. J. D. Lambert, "Vibrational and Rotational Relaxation in Gases", (Clarendon Press, Oxford, 1977).

64. P. F. Zittel and C. B. Moore, J. Chem. Phys. 59, 6636 (1973).

65. J. J. Hinchen, J. Chem. Phys. 59, 2224 (1973).

66. L. L. Poulsen, G. D. Billing, and J. I. Steinfeld, J. Chem. Phys. 68, 5121 (1978).

67. G. D. Billing and L. L. Poulsen, J. Chem. Phys. 68, 5128 (1978).

68. J. Tusa, M. Sulkes, and S. A. Rice, J. Chem. Phys. 70, 3136 (1979).

69. P. Hess and C. B. Moore, J. Chem. Phys. 65, 2339 (1976).

70. J. A. McGarvey, Jr., N. E. Friedman, and T. A. Cool, J. Chem. Phys. 66, 3189 (1977).

71. D. J. Douglas and C. B. Moore, Chem. Phys. Letters, 57, 485 (1978).

72. W. J. Sarjeant, Z. Kucerovsky, and E. Brannen, Appl. Opt. 11, 735 (1972).

73. J. P. Pichamuthu, J. C. Hassler, and P. D. Coleman, Appl. Phys. Lett. 19, 510 (1971).

74. A. Yariv, "Introduction to Optical Electronics", Second Edition, (Holt, Rinehart and Winston, New York, 1976).

75. W. L. Fite in "Chemical Reactions in Electric Discharges", (American Chemical Society, Washington, DC, 1969).

76. J. Heicklen, "Atmospheric Chemistry", (Academic Press, New York, 1976), pp. 4, 103-7.

77. W. S. Benedict, R. Herman, G. E. Moore, and S. Silverman, Can. J. Phys. 34, 830 (1956).

78. D. M. Gates, R. F. Calfee, D. W. Hansen, and W. S. Benedict, "Line Parameters and Computed Spectra for Water Vapor Bands at 2.7μ", NBS Monograph 71 (1964).

79. "CRC Handbook of Chemistry and Physics, 57th Edition", (CRC Press, Cleveland, 1976).

80. R. D. Hudson, "Infrared System Engineering", (Wiley-Interscience, New York, 1969).

81. "The SBRC Brochure" (1979).

82. M. A. Johnson, A. L. Betz, R. A. McLaren, E. C. Sutton, and C. H. Townes, Astrophys. J. 208, 145 (1976).